CODEN:LUTEDX/(TEIE-5546)/1-81/(2025)

Industrial Electrical Engineering and Automation

A Study of Changes in Resistivity of the Semi-Conducting Layers in High Voltage Direct Current Cables

Carl Pettersson

Division of Industrial Electrical Engineering and Automation
Faculty of Engineering, Lund University

A Study of Changes in Resistivity of the Semi-Conducting Layers in High Voltage Direct Current Cables

Author
Carl Pettersson

Company Supervisors
Tommy RE Johansson
Helena Johansson
Supervisor
Morten Hemmingsson
Examiner
Avo Reinap

Thesis submitted for the degree of Master of Nanoscience
Project duration: V months

LUNDS UNIVERSITET

Date: June 2025

Abstract

The resistivity of the semi-conducting material in high voltage direct current cables were studied under a variety of conditions. A wide theoretical background was also created, summarizing previous works within the field and providing useful explanations for the characteristics seen in the results. The semi-conducting material works as a protective shield for the insulation of the cable, protecting it from electrical discharge and excessive electrical field concentrations, both of which can damage the insulation and decrease the lifetime of the cables. Pieces of cable were processed in two different ways to create samples designed for measuring both the inner, and outer semi-conducting layers. Measurements were performed using a four-point probe method over durations of 16 hours.

The resistivity of the semi-conducting layers was studied under many different conditions. These include: varying measuring temperatures, using a constant measuring current instead of a periodic one, repeatedly measuring the same sample, using different types of semi-conducting material, using cross-linked and non cross-linked samples, using alternate sample designs, and measuring under different values of relative humidity. Additionally, the measurements that initiated the creation of this thesis were also recreated.

The experiments produced good results, contributing to a deepened understanding of the behavior of the semi-conducting material under laboratory measurements. The results were discussed, both examining what could be explained from theory and what could come as a result of the methodology. Furthermore, some difficulties with the methodology were also discussed. The ultimate goal of this thesis is to deepen the understanding of the semi-conducting material and improve testing methodology, which in turn could help develop more efficient and cost-effective semi-conducting materials for HVDC cables.

Keywords: HVDC, Resistivity measurements, Semi-conducting materials, CB EBA compounds

Acknowledgments

Firstly, I want to thank my supervisors at NKT, Tommy and Helena. They have made this a very pleasurable experience with enough guidance to succeed with my goals without limiting my freedom and creativity. I also want to thank all of my coworkers at NKT for providing a very welcoming and warm environment. I extend special thanks to some of my colleagues. Siri Stening, for all of her help in conducting measurements at times when I have not been at the office. She has been a great help, conducting the measurements with the efficiency expected of someone 20 years her senior. Her input on other matters has also been greatly appreciated. Jessica Segerby, for her endless patience with all of my questions about even the simplest things. Annette Jartelius for providing me with many of the cables used for sample preparation. Anna Andersson, for her help with some of the more advanced tools required to finish this project. Finally, Julie Fouilloux, for sending me some very exciting samples all the way from Köln.

I also want to thank my supervisor Morten Hemmingsson, my examiner Avo Reinap, and my international coordinator Sabine Richardson for their help with everything administrative. It was a long and cumbersome process but your help kept me sane. I also want to thank Morten and Avo for their help in writing the thesis itself. Their tips have been invaluable

I also want to thank my dear friend Anton Jansson who helped in obtaining some of the papers used in the creation of this thesis. His help has been invaluable in procuring knowledge. I also want to thank my friends Vilhelm Conradi and Lina Vängborg who have always been there to help me out, both during this thesis but also the rest of my studies. Furthermore I also want to thank my friend Isabelle Signe Maj Maria Thord for giving me the confidence to never give up and Hanna Odenius for being there for me when things did not go perfectly. Finally, I also want to thank my parents for their continued support throughout this entire project and for always being there for me.

List of Abbreviations

HV - High Voltage
ISL - Inner Semi-Conducting Layer
OSL - Outer Semi-Conducting Layer
EBA - Ethylene Butyl Acrylate
CB - Carbon Black
SCP - Silver Conductive Paint
SMU - Source/Measure Unit
PTC - Positive Temperature Coefficient
NTC - Negative Temperature Coefficient
SEM - Scanning Electron Microscope
EDS - Energy Dispersive X-ray Spectroscopy

Contents

1 Introduction and Background **1**
1.1 Historical Development of HV Cables . . . 1
1.2 Design of HV Cables . . . 2
1.3 The Semi-Conducting Layers . . . 3

2 Introductory Experiments and Purpose of Thesis **5**
2.1 Previous Measurements . . . 5
2.1.1 Methodology . . . 5
2.1.2 Results . . . 6
2.1.3 Discussion of Results . . . 7
2.2 Purpose of Thesis and Aim . . . 8
2.2.1 Scope of Study . . . 8
2.2.2 Limitations . . . 9

3 Theory **10**
3.1 Purpose of Semi-Conducting Layers . . . 10
3.2 Design of the Semi-Conducting Material . . . 12
3.2.1 Electrical and Thermal Properties of Carbon . . . 12
3.2.2 Polymers and Ethylene Butyl Acrylate Copolymer . . . 13
3.2.3 The Semi-conducting Compound and its Production . . . 13
3.3 Mechanics of Electrical Transport in the Semiconducting Compound . . . 14
3.3.1 Percolation Theory . . . 15
3.3.2 The Effect of Temperature on Resistivity . . . 17
3.4 Electrical Characterization . . . 18
3.4.1 Contact Resistance . . . 18
3.4.2 Previous Examples of Electrical Characterization of CB and Polymer Compounds . . . 19

4 Methodology **22**
4.1 Preparation of Sample . . . 22
4.2 Resistivity Measurements . . . 25
4.2.1 Recreation of Introductory Results . . . 26
4.2.2 Repeated Measurements . . . 26
4.2.3 Constant Injected Current . . . 27
4.2.4 Temperature . . . 27
4.2.5 Different Types of Semi-Conducting Layers . . . 27
4.2.6 Non Cross-Linked Samples . . . 27
4.2.7 Different Shapes of OSL-Samples . . . 27

4.2.8 Humidity 28
4.3 Temperature Measurements 29
4.4 Optical and Chemical Characterization 30

5 Results and Discussion **31**
5.1 Recreation of Introductory Results 31
5.2 Repeated Measurements on One Sample 33
5.3 Constant Measuring Current 35
5.4 Temperature Effects 36
5.5 Different Types of Semi-Conducting Layers 43
5.6 Cross-Linking 43
5.7 Alternate OSL Design 45
5.8 Humidity Effects 46
5.9 Optical and Chemical Characterization 47
5.9.1 Contaminants and Chemical Characterization 48
5.9.2 Imaging of Contacts 53
5.10 General Discussion of Results and Error Analysis 55

6 Conclusion **60**

7 Outlook **61**

8 Confidentiality, Conflicts of Interest, and Ethical Disclosure **63**

1 Introduction and Background

In an increasingly electric world, the efficient transmission of electricity becomes more and more important. As the need for power increases one faces the options of either increasing the current or voltage. Increasing current requires larger conductors and leads to more joule heating. Increasing voltage, on the other hand, still increases the power transmitted but with a lower current. This leads to fewer losses and makes increasing voltage, instead of current, the clear choice when it comes to scaling up power [1]. Some difficulties do come as a consequence of increasing voltage as it puts larger demands on the insulation system. Over long distances, electricity is transferred using high voltage, HV, cables which are quite efficient with minimal losses [2][3][4].

HV cables can be divided into two main categories: overhead power lines and ones that are buried either underground or placed on the seabed. For suspended cables, the surrounding air works as both a good insulator and cooling medium [5]. Due to this, these cables are generally easier and cheaper to design and manufacture compared to submerged cables that require an added insulation layer as well as a semi-conducting layers to electrically protect the insulation layer [6][7].

1.1 Historical Development of HV Cables

HV cables have gone through many iterations since their conception. The origins of HVDC cables date back nearly 150 years to 1879, when Thomas Edison wrapped three copper wires with rope, encased them in a steel pipe, and filled the pipe with asphalt. This cable was able to transmit voltages of 220 V [8][9][10]. Around ten years later, in 1890, Sebastian Ziani de Ferranti designed a cable with waxed paper insulation, capable of transmitting 10 kV. Paper cables were further developed in 1924 by Luigi Emanueli who impregnated the paper with fluid oil. This significantly improved stability and allowed the cables to transmit voltages of up to 132 kV, which was then further improved upon in the following years, culminating with voltages of 220 kV twelve years later [11]. The next big improvement came in 1942 when synthetic plastics was first used. Marking a shift towards the cables we see today. New synthetic materials kept being developed such as ethylene propylene rubber in 1955 and cross-linked polyethylene (XLPE) in 1963 further improving insulating abilities and stability. Synthetic insulation cables have since then become increasingly common, phasing out oil impregnated paper cables. More recent improvements have been seen in 2000 which saw the first long-distance 500 kV XLPE cable. Multiple international projects have since then been conducted, connecting energy infrastructure between different countries. In 2022 a 525 kV DC cable was successfully developed, doubling power transmissions over long distances [12]. As the need for sustainable energy grows, advancements within cable technology seem inevitable.

It is impossible to discuss the evolution of DC cables without mentioning the so called "War of currents". Towards the end of the 19th century, proponents for AC and DC transmission systems competed to establish their system as the dominant one. Eventually, AC came out as the winner and has since then been the predominant method of electrical power transmission [13]. In recent years, however, some flaws with AC have become apparent. DC cables have a couple of advantages such as: their superior ability to transfer energy over long distances, the ability to interconnect different grids at different frequencies, and their applications when it comes to renewable energy such as wind, and solar power [14][15][16]. This does not, however, mean that DC is strictly better than AC. AC still has advantages with a large one being the ease at which one can either increase or decrease the voltage using transformers. Another benefit is that most electrical generators generate AC power with some clear exceptions being solar plants and windmills [17]. These differences are also why larger grids sometimes use combinations of AC and DC. Although converting AC to DC results in losses it could still be preferential compared to the losses from long distance AC power transfer [18].

1.2 Design of HV Cables

The design of submerged cables naturally vary, but in general they have the same basic components in common, both for AC and DC cables [19][20][21]. These being, from the middle outwards (Figure 1.1):

1. The conducting core/cable
2. Swelling bands with superabsorbent polymer powder
3. Conductor bands
4. A thin semi-conducting layer
5. A thick insulating layer
6. A thin semi-conducting layer
7. Swelling bands and superabsorbent polymer powder
8. A protective jacket, consisting of a metal sheath and an oversheath

An image, obtained from Severengiz, Sprenger, and Seliger [19], showing the structure, and main layers, of a typical HVDC cable can be seen below in Figure 1.1 along with short descriptions of each layer in Table 1.1.

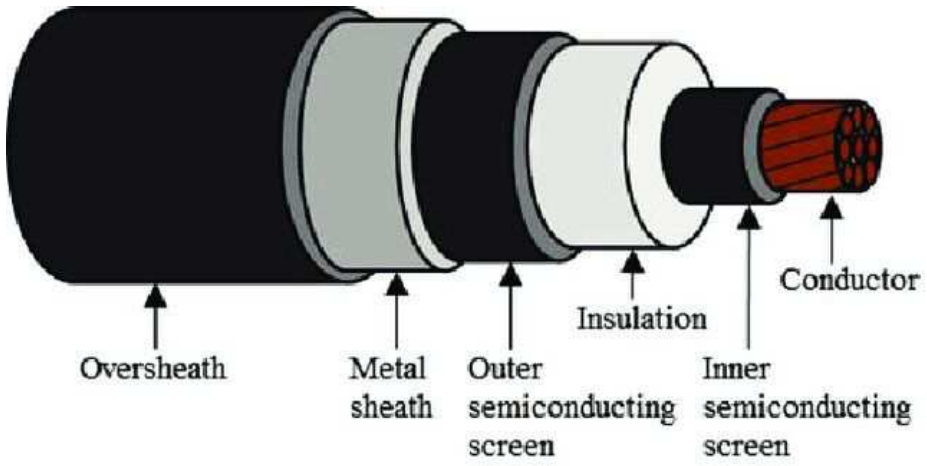

Figure 1.1: Image showing the structure, and main layers, of a typical HVDC cable. Image taken from Severengiz, Sprenger, and Seliger [19].

Table 1.1: Table describing the different layers of a HV cable and their purposes.

Layer #	**Name**	**Purpose**
1	Conducting core	Conducts current
2	Swelling bands and superabsorbent polymer powder	Protects the conductor from moisture
3	Conductor band	Protects the swelling bands
4	Inner semi-conducting layer (ISL)	Protects the insulation from electrical stress and removes the risk of electrical discharge
5	Insulation	Electrically isolates the conductor
6	Outer semi-conducting layer (OSL)	Further protects and shields the insulation from electrical stress
7	Swelling bands and superabsorbent polymer powder	Protects the outer semi-conducting layer from moisture
8	Protective sheath	Protects the cable from physical and chemical damage

1.3 The Semi-Conducting Layers

The main layers of an HVDC cable that are of interest for this work are the semi-conducting layers. Both the inner semi-conducting layer, ISL, and the outer semi-conducting layer, OSL. Normally, in cables used for lower voltages, these layers are not required. When

using voltages above approximately 2 kV the extra semi-conducting layers become necessary to protect the insulation from electrical damage [22]. The semi-conducting layers serve multiple purposes, all extending the lifetime and stability of the cables. Without them, electrical stress-induced breakdowns of the insulation can occur [23][24]. The semi-conducting layer also reduces the risk of electrical discharge and provides a good interface between the conductive core and the insulation [25][26].

For the semi-conducting layers to be able to handle these tasks they have to fulfill a couple of criteria. They have to have similar mechanical and thermal properties to the insulation. They also have to have a resistivity between that of a conductor and insulator. The exact resistivity values naturally depends on factors such as the use cases of the cable, the voltage to be transmitted, whether it is an ISL or OSL, and the temperature when measuring the resistivity, but typical values range around 1-100 Ωm at 90 $^{\circ}C$ [27][28]. A resistivity that is too small, i.e. too conductive (as an exaggerated example), leads to the semi-conducting layer essentially becoming an expansion to the conductor, increasing leakage current and leading to excessive joule heating, damaging the insulating layer. On the other hand, if the resistivity is too high, i.e. not conductive enough, the semi-conducting layer essentially just acts as more insulation. This leads to the same damage that would be seen if there was no semi-conducting layer, that is electrical discharge and stress.

Since the semi-conducting layers are clearly an integral part of the electric insulation system of a working HV cable it is important to understand how they are affected by different environmental factors that they could normally encounter. For this thesis the main attribute of the semi-conducting layer that will be studied is its resistivity.

2 Introductory Experiments and Purpose of Thesis

This thesis was developed in collaboration with the material laboratory division at NKT. This chapter details measurements that had been previously performed at the division before the MSc thesis which sparked interest in further investigations and laid the foundation for this project. The methodology of these measurements are described, the results shown, and subsequently discussed.

2.1 Previous Measurements

In these previous measurements, oddities were detected in 24-hour long measurements of the resistivity in the semi-conducting layer. Measurements showed changes in resistivity by up to a factor of 50 over the span of a couple of hours, reaching values above 1000 Ωm, larger than what internal guidelines allowed. The internal guidelines allows ISL samples to have a resistivity of < 1000 Ωm and OSL samples < 500 Ωm. This type of measurement, that was performed over multiple hours, was not something that had previously been done at the division. These results were also something that was only seen in measurements at the lab and not in actual usage of the cables.

2.1.1 Methodology

Two types of samples were created to measure either the ISL or OSL. These were created in accordance to IEC standards 60840 § 12.4.9, 62067 § 12.4.9, 60811-401 and internal guidelines of the Material Technologies division at NKT. A sketch showing the design of the samples can be seen below in Figure 2.1.

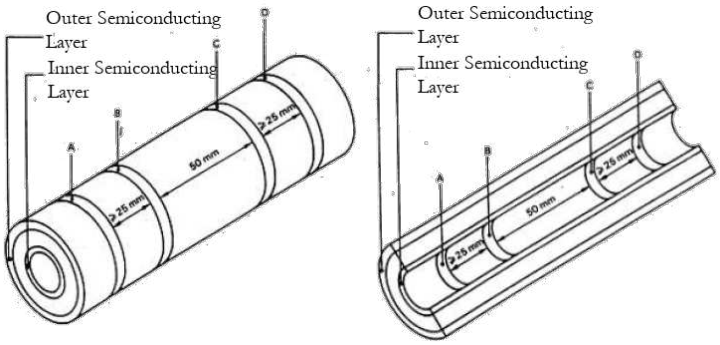

Figure 2.1: A sketch showing the designs of both ISL and OSL samples along with the placements of the measuring electrodes. The inner and outer semi-conductor layers are also marked.

Room temperature samples were put in an oven at the standard measuring temperature of 90 $°C$. The resistivity was measured when the cable was first inserted into the oven, followed by a measurement after 15 minutes, 30 minutes and then every 30 minutes onward for a duration of 8 hours. A final measurement was performed 24 hours after the initial one.

2.1.2 Results

The introductory measurements that initiated this project can be seen below in Figure 2.2.

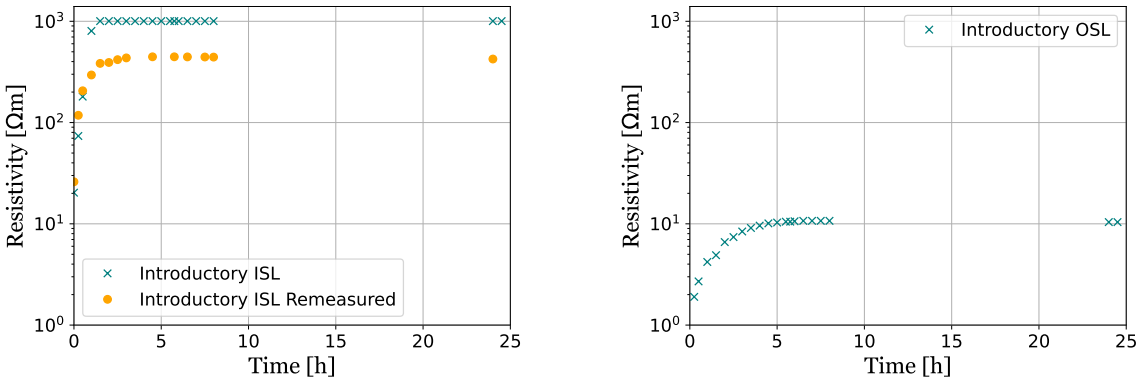

(a) Some of the ISL resistivity measurements that initiated the creation of this thesis.

(b) One of the OSL resistivity measurements that initiated the creation of this thesis.

Figure 2.2: Some of the resistivity measurements that initiated the creation of this thesis. These graphs show how the resistivity of the ISL can change by up to a factor of approximately 50 over the span of just a couple of hours. They also shows how the ISL and OSL can exhibit very different characteristics.

As can be seen in Figure 2.2a, the resistivity changes from around 20-40 Ωm to above 1000 Ωm within the span of just one hour, exceeding the upper allowed limit of 1000 Ωm for the inner semi-conducting layer. Even in the re-measurement of the ISL layer it reaches a resistivity above 500 Ωm. This resistivity change is not as extreme for the OSL, but a change of a factor ≈ 20 over a couple of hours can still be seen. For the ISL, the measured values exceeded the tools upper limit of 200 $k\Omega$ which is why it flattens quickly and remains unchanged for most of the measurement. It was therefore remeasured. Similarly to the ISL measurements, a strong increase in resistivity is seen during the first couple of hours of the OSL measurement before a steady state is reached. The main differences between the ISL and OSL results are the time it takes for the measurements to reach a steady state and the final resistivity values. ISL samples reach their steady state quicker but also have much higher resistivity values.

2.1.3 Discussion of Results

The resistivity goes through two distinct regions, a transitionary and stable region. Initially, one can see a strong increase in resistivity that starts slowing down after a while. This behavior resembles an exponential function and can be explained by the resistivity increasing as the sample heats up. As the sample approaches the measuring temperature, the speed at which the sample heats up decreases, explaining the deceleration of the resistivity. The same behavior can be seen for both ISL and OSL samples but over a much longer amount of time for the OSL sample. This could quite simply be explained by the vastly different masses between the ISL and OSL samples, with the OSL sample's larger mass leading to a slower increase in temperature.

After $\approx$ 3 and $\approx$ 6 hours for ISL and OSL samples respectively the resistivity starts plateauing, reaching a steady state. A relatively minor, continuous, decrease of resistivity can however be seen after leveling off. This can more clearly be seen when looking at the raw data used for the graphs which is displayed below in Table 2.1. One can see that for every column (with an exception of the first one in which there was an error with the measuring device) there is a clear drop in resistivity between the 8 and 24 hour measurements. One can also see that the resistivity seems to peak somewhere around 3-7 hours after which it starts slowly decreasing.

Table 2.1: Data used for the creation of the graphs in Figure 2.2.

Time [h]	**Resistivity ISL [Ωm]**	**Resistivity ISL [Ωm] Remeasured**	**Resistivity OSL [Ωm]**
0	20.3	2.6	0.7
0.25	73.7	11.9	1.9
0.5	180.3	20.5	2.7
1	803.0	29.5	4.2
1.5	1004.2	38.4	4.9
2	1004.2	39.2	6.6
2.5	1004.2	41.8	7.4
3	1004.2	43.5	8.4
3.5	1004.2		9.1
4	1004.2		9.6
4.5	1004.2	44.6	10.1
5	1004.2		10.3
5.5	1004.2		10.5
5.75	1004.2	44.6	10.5
6	1004.2		10.6
6.5	1004.2	44.5	10.7
7	1004.2		10.7
7.5	1004.2	44.4	10.7
8	1004.2	44.3	10.7
24	1004.2	42.4	10.4
24.5	1004.2		10.4

2.2 Purpose of Thesis and Aim

Volume resistivity measurements are a common and efficient way of ensuring the properties of the material. It is therefore important to have a good understanding of what effects and characteristic behaviors can be seen in the semi-conducting material during these types of measurements.

This thesis aims to provide a detailed overview of how the semi-conducting layers behave during long measurements, with durations of a couple of hours, under different measuring conditions. It also aims to provide a large theoretical background of how the semi-conducting material works. With the theoretical background, the phenomena seen in the measurements can be understood and explained with greater accuracy.

The ultimate goal of the thesis is to help provide a better understanding of the testing methodology, the semi-conducting material, and how they relate to each other. This can then help develop more efficient testing methods that, in turn, help out with developing more efficient materials for cheaper and better cables.

2.2.1 Scope of Study

There are many different aspects to the cables that can be studied. It is therefore important to be clear about what variables we vary and which we keep constant. Furthermore, it is also important to note which factors that can unintentionally vary as a result of which samples that are used.

Tests will be performed at varying temperatures centered around the standard measuring temperature of 90 $^{\circ}C$. Measurements will also be performed in climate chambers at different humidity values. Recreations of the previously discussed results, using the same type of cable, will also be done. Measurements will also be performed using different types of semi-conducting materials, using a constantly applied measuring current and a periodically applied measuring current, as well as repeatedly measuring on the same sample. Finally samples that have been cross-linked and not cross-linked will be compared.[1] Optical and chemical characterizations of the samples and contaminants will also be performed using a SEM equipped with an EDS.

This thesis will also provide a solid theoretical background of the current-transport mechanisms present in the semi-conducting layer of HV cables, along with detailed descriptions of potential errors that can occur during regular measurements, so that measures can be taken and make sure that future measuring endeavors and research will be more successful.

This thesis does not seek to examine these aforementioned conditions for cables under regular use, but rather specifically within a laboratory context where the material is ex-

[1] Cross-linking is a chemical process that increases form stability and temperature resistance of a polymer. As a default all samples are cross-linked.

amined. The conditions that some of the measurements are performed under would also never reasonably occur for regular cables.

2.2.2 Limitations

Due to the length of each measurement and the large amount of variables examined there are some potential limitations to the depth and consistency of these results. All measurements are backed up by either one or two other measurements performed using similar samples and under the same conditions. This should make sure that all results are accurate but they would naturally be more precise with more measurements reinforcing them. There are also limitations concerning the available samples. Not all samples can be taken from the same length of cable, which could potentially affect the results. Care will, however, be taken to make sure that all samples are similar and consist of the same material (unless a different material was to be studied). The main difference in this case would be the mass of the samples which could potentially change the way that the sample reacts to, for example, heat.

3 Theory

This chapter goes into more detail about the purpose and design of the semi-conducting layers. It also describes how well, and in which way, the semi-conducting layer conducts a current. How resistivity is calculated, along with previous studies on similar topics to the ones covered in this thesis are also included.

3.1 Purpose of Semi-Conducting Layers

HVDC cables consist of multiple layers with different purposes. These are detailed and described in Figure 1.1 and Table 1.1. A crossectional picture of one of the cable samples used for this thesis can be seen in Figure 3.1.

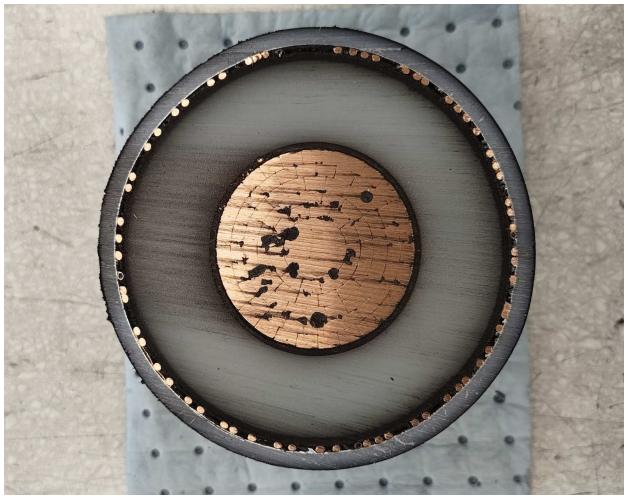

Figure 3.1: Crossectional image of one of the cables used for this thesis.

For this study, the protective jacket is always removed as it is not relevant. Its main purpose are to protect the cable from outside mechanical and chemical impacts [29], neither of which are applicable for this project. This thesis focuses on the inner- and outer semi-conducting layers. These layers, that are not present for cables of lower voltages (roughly below 2 kV [22]), serve the purpose of protecting the insulating layer from both electrical discharge and overwhelming electric stress. Without the semiconducting layers, prolonged safe use of the cables is not possible without degradations in the quality of insulation [30].

The conductive core itself consists of multiple wires that are twisted together. This results in an uneven conductor surface that causes the electrical fields from each individual wire

to interact with the other electric fields in a way that creates "hot-spots". In these regions, the concentration of electric fields are much higher compared to other parts of the cable [31]. The high voltages transmitted through the cable result in an electric field strength that can exceed the dielectric strength of the insulation, especially at the hot-spots.

Without the ISL, these concentrations of electric fields could result in large amounts of electrical stress on the insulating layer, leading to malfunctions and electrical breakdown [31]. The equipotential semiconducting layer redistributes the electrical stress evenly in the insulator, removing these dangers and ensuring the insulation layers integrity [25]. A sketch showing this can be seen below in Figure 3.2.

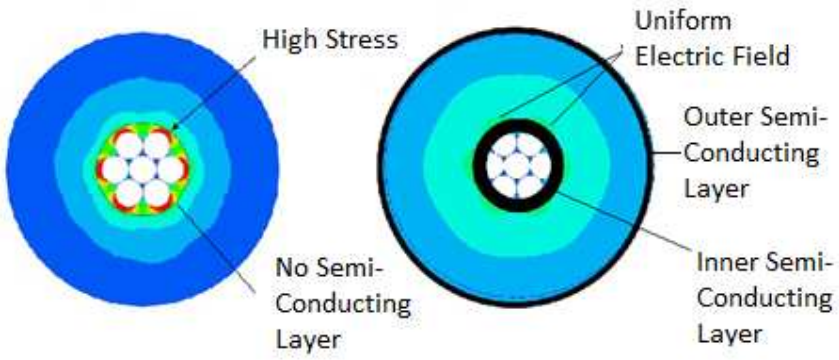

Figure 3.2: A sketch from [31] showing how a lack of semi-conducting layers lead to high stress regions. The sketch has been modified to have clearer text and an explicitly marked outer semi-conducting layer.

There is also the matter of air gaps that are formed between the insulator and conducting layer. Without the ISL electrical discharges between the conductive core and the insulating layer can occur [32]. These discharges can also decrease the integrity and longevity of the insulating layer [26][33].

The OSL fills a similar purpose. Acting as a grounding surface, it helps to spread out the electrical stress evenly throughout the insulator and prevents electrical discharge between the insulator and the outer jacket. It also provides a nice interface between the insulation and the protective sheath, reducing potential mechanical stress which could reduce the insulation capabilities of the insulation layer [34][35].

For the semi-conducting layer to fulfill these requirements the material has to have a couple of attributes. It requires a resistivity such that it can stop accumulation of charge but not high enough to be completely conductive, a sufficient flexibility and moldability, a good compatibility and interface with the insulation material, and good thermal stability [36]. To fulfill these criteria a carbon black (CB) blended polymer compound is employed. An example of one type of semi-conducting compound that fits all of these criteria, and the one

that is used in the cables looked at in this thesis, is an Ethylene Butyl Acrylate Copolymer (EBA) blended with CB [37][38][39].

3.2 Design of the Semi-Conducting Material

As mentioned in section 3.1, the semi-conducting material is a compound of EBA copolymer and CB. To understand how these work together to form a semi-conducting material they will be individually described first.

3.2.1 Electrical and Thermal Properties of Carbon

Carbon is a material that can appear in many different configurations, each with their own set of electrical and thermal characteristics. Common variations of carbon are those of diamond and graphite. These are very different when it comes to resistivity, ρ. Diamond structures have high values of resistivity $\rho \approx 10^{18}\ \Omega m$ while graphite structures have low values of resistivity $\rho \approx 8\ \mu\Omega m$ [40][41]. A third type of carbon is amorphous carbon, which is slightly more difficult to describe in a general fashion.

Amorphous carbon, as the name implies, can be regarded as an amorphous material, meaning that it has no long range order. Generally, it is either found as a powder or deposited on a thin film [42]. Although no long range order is observed, there is still short range order, forming shapes similar to that of graphite.[1] Due to this, amorphous carbon has a resistivity closer to graphite than diamond, although this naturally also depends on the purity of the carbon and how it has been treated among other factors.

For the purpose of creating the semi-conducting layer it has to fulfill a couple of requirements. It needs to have a low resistivity, be durable, and be easily mixable into the polymer. Carbon black, which is a type of powdered amorphous carbon, mostly fits these criteria but with a slightly too large resistivity. To further reduce the resistivity to the desired level, the CB undergoes a graphitization procedure. This increases the amount of graphite-like ordered structures which in turn decreases resistivity [43]. Graphitized CB can reach resistivity values as low as $\rho \approx 2 \cdot 10^{-3}\ \Omega m$ [44]. The durability and mixability of graphitized CB remains sufficient as the graphitization only affects short range order of the CB and not its powdered nature. Due to these factors, graphitized CB is common when designing the semi-conducting layer.

[1] Long range order in a material refers to some overlying structure throughout the material, typically in the form of a crystal lattice. Short range order means that there are local clusters of structured atoms but that the material as a whole does not have a symmetrical structure. Most metals and semi-conductors exhibit long range order, amorphous solids and liquids short range order, and gases no order.

3.2.2 Polymers and Ethylene Butyl Acrylate Copolymer

A polymer is a repeating pattern of chemically bonded, smaller monomer units. These monomers can be varied in both size and complexity which also leads to the same being true for polymers [45]. Polymers are used in a lot of different areas, with some more everyday examples being plastic, rubber, and many proteins in the body. Due to the very broad definition of what a polymer is, it is not surprising that polymers can also exhibit many different electrical characteristics. The previously mentioned example of rubber, is a clear example of an electrical insulator polymer with a resistivity of $\approx 10^{13}\ \Omega m$ [46]. Polymers can, however, also act in other ways such as: dielectrics, semiconductors, metal-like conductors, and even superconductors [47].

The polymer used in the semi-conducting compound is Ethylene Butyl Acrylate Copolymer (EBA). This copolymer is itself an insulator, but it has many aspects that make it a good candidate for the semi-conducting compound. Due to its nature of an insulating polymer, it creates a nice interface with the insulating layer, reducing mechanical stress. It also has good thermal stability, bondability to different substrates, flexibility, and low water absorption [48][49]. As EBA is a copolymer, one can also vary the proportions of the different monomers to vary its properties and adjust it for its desired use.

Another relevant aspect of polymers is that of cross-linking. This is a process by which multiple polymer chains are linked together, either through covalent or ionic bonds [50]. There are various methods to create these bonds, including by irradiation, chemical reactions, and thermal treatments [51][52][53]. Cross-linking has many effects, with some examples being: reducing mobility of polymer chains, in turn increasing temperature resistance, increasing molecular weight, and improving form stability [54][55].

3.2.3 The Semi-conducting Compound and its Production

The semiconducting compound is a mixture of EBA and CB. The polymers insulating capabilities and the CB's good conductivity gives the resulting compound its desired resistivity, $\rho \approx 10^{-1} - 10^{6}\ \Omega m$ [56]. This span of resistivity is quite large and can be adjusted by changing the proportions between the components. If too little CB is added then the resistivity will remain mostly unchanged from the insulator resistivity, resulting in the semi-conducting compound essentially just being more insulator [57]. On the other hand, if too much CB is added, the semi-conducting compound will lose its flexibility and interface with the insulation layer [58]. It is important to note that this desired concentration is not constant throughout all semi-conducting materials, but instead depends on the usage of the material, the type of CB, the type of polymer, and the mixing of the two [59][60][61].

The two most important things that have to be considered when creating the semi-conducting compound are: to obtain a good mixing of the CB such that is somewhat homogeneously distributed throughout the compound and to preserve the structure of both the conductive material and the polymer [36]. The CB's conductivity largely comes

from its graphite structure, and if this structure is damaged during the mixing process, it could immensely increase the resistivity of the compound. Similarly, without a somewhat homogeneous distribution of CB in the compound long range current transport would be impossible, once again severely increasing resistivity.

This semi-conducting compound does not conduct electricity in the same way as normal semi-conductors like Si and Ge, which is also why it is referred to as a semi-conducting material and not a semi-conductor. Normal semi-conductors conduct electricity via the excitation of electrons from the valence band to the conduction band. The EBA CB compound, on the other hand, conducts electricity mainly through physical connections of CB and the tunneling of electrons between different CB patches [62][63][64].

3.3 Mechanics of Electrical Transport in the Semiconducting Compound

Materials can generally be grouped into three main categories when it comes to conducting electricity: conductors, semi-conductors, and insulators. In conductors, the abundance of free electrons move freely through the material, allowing electric current to flow easily. In contrast, semi-conducting materials lack a large number of free electrons, instead current flows when electrons gain enough energy to jump from the valence band to the conduction band. Electrons in the valence band are bound to atoms and therefore do not conduct electricity, while those in the conduction band are free to move and contribute to electrical conduction. Insulators are similar to semi-conductors in the way that they can normally only conduct when electrons in the valence band get excited to the conduction band, with the key difference being the larger band gaps of insulators making the excitations less likely [65].

Conductors, semi-conductors, and insulators each respond differently to changes in temperature. In general, the resistivity of conductors increases with increasing temperatures, while the resistivity of semi-conductors and insulation decrease. For conductors, the energy of the free electrons increases with temperature, causing them to increasingly collide with each other, increasing resistivity. On the other hand, in semi-conductors and insulation, the increase in electron energy causes more electrons in the valence band to get excited to the conduction band, thus decreasing resistivity [66].

The conduction in the semi-conducting compound can not be described using band theory in the way that typical semi-conducting materials can be. Instead, multiple other models, among which percolation theory and quantum tunneling, are used to describe how current is transported. This area has been widely studied, with the effects that CB type, CB concentration, and polymer type, among others, have on conductivity having been discussed [67][68][69][70].

3.3.1 Percolation Theory

Percolation theory describes the transport properties of a system with clusters capable of transporting something dispersed in a larger network of non-transporting material [71][72]. It is applicable in a large amount of areas including, but not limited to, fluid movements through porous materials, artificial neural networks, and even social dynamics such as the spreading of rumors [73][74][75].

For the purpose of this thesis, percolation theory works as an effective way to describe the current-transportation of the clusters of conductive CB throughout the insulating EBA copolymer [76][77][78]. Percolation theory describes how at a certain CB concentration threshold, conduction will change from being localized within local CB clusters, to spanning the entire material by long range transport between CB clusters [79]. This concentration threshold, called the percolation threshold, depends on many factors such as the quality, composition, and electrical characteristics of both the CB and polymer, along with the effectiveness of mixing [80][81][82]. When the threshold is reached, the conductive abilities of the compound increase significantly, as there is enough CB at appropriate positions, to allow for long range transport of currents. This phenomenon has been widely documented through both theoretical and experimental work, with the changes of resistivity at the percolation threshold having a magnitude of around $10^{12} - 10^{16}$ Ωm. This does, however, naturally depend on which materials were used [76][77][78][83][84].

At low CB concentrations, below the percolation threshold, current transport is local and does not occur throughout the entire material, leading to a very high resistivity. Current is locally transported in two ways. One way is that of hopping, or tunneling, between conductive islands (CB clusters), through surrounding potential barriers (the insulating polymer matrix) [62][63][64][85][86]. There is also that of regular current transport by physical connections throughout CB agglomerates.

As the concentration of CB increases, the average distance between the conductive islands decreases which in turn increases tunneling probabilities [87]. When the percolation threshold is reached, long range transport starts being seen, significantly decreasing the materials resistivity [88].

Increasing the CB concentration past the percolation threshold does relatively little to affect the resistivity. The paths that the current takes through the material have already appeared and further increases to CB concentration simply increases the amounts of available routes that the current can take. At even larger CB concentrations tunneling becomes less relevant as larger and longer geometric paths become available [89]. The problem with CB concentrations that are too large, is as previously mentioned, the worsened mechanical and interfacial properties of the semi-conducting material.

There is an important distinction here to make regarding the percolation threshold. It describes the concentration of CB required to see long range transport of currents throughout the entire material. What is not included in this description is whether the conducting

path has to physically touch or not. As previously discussed, hopping/tunneling is a common mechanism of current transport which does not require the CB to form a continuous, physical, network for current to be transported [62][63][64]. For materials consisting of agglomerates of CB particles spread throughout the polymer it is reasonable to consider the percolation threshold the point where these conductive clusters are sufficiently close to lead to high-probability tunneling throughout the entire material [90]. There are, however, other types of CB filled polymers where the CB stretches out in narrow, long, well connected bands. For these materials there is relatively little current through tunneling and most transport happens through physical connections [91]. There are even ways of treating the semi-conducting material in ways that make long range physical connections are the main driver of conduction while still having low percolation thresholds of ≈ 1 % [92]. Simply put, the structure, placement, and type of CB in insulation matrices can vary greatly, leading to very different characteristics of which transport mechanisms are relevant and at what CB concentration the percolation threshold is found [93][94].

The prevalence of the different transport mechanisms also depend on the temperature of the material. As the temperature increases, differences in the polymer and CB's thermal expansion coefficients cause them to expand different amounts. This mismatch can cause physical connections to get severed and distances between CB clusters to increase [91], both causing an increase in resistivity. Even if a physical connection has gotten severed, current can still flow via tunneling. As a result, tunneling becomes increasingly dominant as the material heats up.

The aforementioned increase in distance between conductive clusters gives a strong increase in resistivity. This is, to a big part, due to the probability of quantum tunneling decreasing. A decreased tunneling probability essentially means that fewer electrons travel throughout the material which is analogous to an increased resistivity. This thesis will not go into too much detail regarding quantum tunneling probabilities but a short summary is in order.

Quantum Tunneling Through a 1D Potential Barrier

Quantum tunneling allows a particle, such as an electron, to pass through a potential barrier that it classically would not have enough energy to pass through. A typical analogy would be that of kicking a football up a hill. If the ball (the electron) is kicked with enough kinetic energy to overcome the potential energy at the top of the hill (potential barrier) it would be able to roll to the other side. If the ball does not receive enough energy it will simply roll back down the hill. When considering an electron on a CB cluster (the football) trying to pass through the potential barrier of the polymer (over the hill) this does not hold. As a consequence of the electrons wave function having to be continuous throughout, and at the edges of the barrier, the electron has a finite probability to travel to the other side of the barrier without having enough energy to pass over it. This would be analogous to the ball making it up partway to the top of the hill and then appearing on the other side. The probability of this happening depends on three main factors: the

height of the potential barrier, the energy of the electron, and the width of the barrier. Tunneling becomes more likely as the electron's energy approaches the barrier height, but less likely as the barrier width increases. Tunneling probability, T, can be described by the following equation:

$$T \approx e^{-2w\sqrt{\frac{2m(U_0-E)}{\hbar^2}}} \tag{3.1}$$

where w is the width of the barrier, U_0 the height of the barrier, E the energy of the particle, m the mass of the particle, and $\hbar$ the reduced plank constant [95][96]. Examining this equation it becomes clear that the width of the barrier matters most when it comes to tunneling probability.

3.3.2 The Effect of Temperature on Resistivity

As the resistivity of the semi-conducting material increases with increasing temperature it is said to have a positive temperature coefficient (PTC). The increase in resistivity primarily come from the severing of physical connections and the increasing distances between CB clusters as the semi-conducting material approaches its glass transition temperature, around 70 $°C$. An increase in distance between clusters, i.e. an increase in width for Equation 3.1, causes an exponential drop in tunneling probability [91]. On the other hand, electron energies also increases with temperature, in turn exponentially increasing tunneling probability. Increases in distance between clusters is the most impactful out of these two competing effects. Increases to tunneling probability correspond to decreases in resistivity.

As the material reaches higher temperatures, around 100 $°C$, another phenomena is seen where the resistivity starts decreasing again. This negative temperature coefficient (NTC) is not yet completely understood but seems to come from reaggregation of conductive particles and conductive pathways being rebuilt [97][98].

Cross-linking

Cross-linking, as described in section 3.2.2, increases the temperature resistance and form stability of the polymer. Cross-linking has two primary effects on resistivity. At room temperature cross-linking raises the potential barrier height, very slightly decreasing tunneling probability, and amplifying resistivity. This, however, only holds for semi-conducting materials where tunneling is the main current-transport mechanism at room temperature. If physical conduction paths are also present, cross-linking does nothing to increase resistivity. The second effect of cross-linking is seen at larger temperatures. Due to the increased temperature resistance and form stability of the polymer it is not as affected by breaking down of conductive paths as non-cross-linked materials and therefore sees a smaller PTC.

3.4 Electrical Characterization

Calculating the volume resistivity, ρ, is quite simple. It can be found by a simple relation between geometric properties and the measured resistance.

$$\rho = R\frac{A}{l} \tag{3.2}$$

As the measured samples are sheaths of a cylinder the area is given by $A = \pi(d-t)\cdot t$ where d is the outer diameter of the sheath and t is the thickness of it. l shows the distance between the probes over which the resistance is measured. Putting the adjusted area expression into the previous equation gives the following

$$\rho = R\frac{\pi(d-t)\cdot t}{l} \tag{3.3}$$

with a factor of $\frac{1}{2}$ if half a cylinder is measured.

Resistance, and in turn resistivity, both have a clear dependence on temperature and can be described by the following equation.

$$R = R_0\left(1+\alpha\left(T-T_0\right)\right) \tag{3.4}$$

Making the assumption that the area and length remain unchanged (which is mostly correct) allows Equation 3.4 to be rewritten for ρ.

$$\rho = \rho_0\left(1+\alpha\left(T-T_0\right)\right) \tag{3.5}$$

3.4.1 Contact Resistance

Something that has to be considered when doing resistance measurements is contact resistance. It is normally one of the most common causes for poor or inaccurate measurements. Contact resistance occurs as a consequence of properties of the interface between the measuring equipment and the sample. Examples of these properties are: the conductivity and geometric features of the electrode, the physical contact between the probe and electrode, and possible contaminates [99][100][101].

As part of preparing the samples for electrical measurements, contacts are created using thin layers of silver paint that are painted along the semi-conducting area. The extreme conductivity of silver makes it a good electrode to reduce contact resistance [102][103]. The silver paint only consists of somewhere between 30-70 % but this does not really affect its efficiency [103][104]. At elevated temperatures the acetone mixed into the silver paint also evaporates, increasing the silver concentration. Furthermore, by painting the electrode along the entire sample, using a sufficient thickness, and making sure that a good coverage is reached, contact resistance can be further decreased [105].

As measurements are performed at high temperatures, around 90 $°C$, and over long periods of time it is important to note how these factors affect contact resistance. As the contacts are made of silver, being a noble metal, the risk of oxidization and other reactions are quite low. Adsorbent films can, however, still form which, in turn can increase contact resistance [87]. Although silver-oxygen reactions are unlikely, silver-sulfur reactions are a more valid concern. These could lead to degradation in contact quality [106][107]. Sulfur is a common element for cross-linking rubbers, [108], but should not really be seen in any significant quantities post cross-linking.

3.4.2 Previous Examples of Electrical Characterization of CB and Polymer Compounds

Multiple previous studies that have examined the electrical properties of the semi-conducting material that makes up the semi-conducting layers in HV cables. Many of these have focused on the resistivity as a function of the CB volume concentration. The resistivity starts at large, insulating values when the CB concentration is low, but as the concentration increases it eventually reaches the percolation threshold and a rapid decrease in resistivity follows. Below in Figure 3.3, taken from [109], one can clearly see this drop in resistivity. Note that the x-axis is normalized against the percolation concentration, ϕ_c, which is at $\approx 9 - 11$ %.

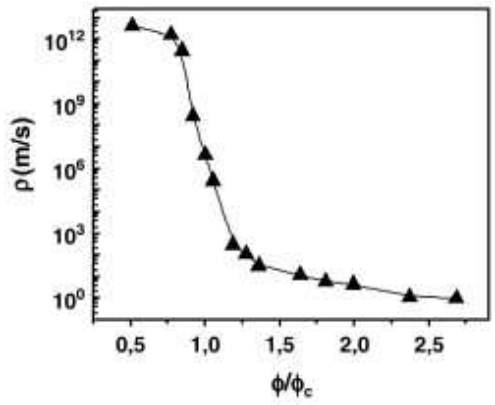

Figure 3.3: "Electrical resistivity of EBA/CB copolymer composites, at ambient temperature. Solid line is drawn to guide the eyes only." The x-axis shows ratio of the amount of black carbon to the percolation threshold at $\approx 9 - 11$ %. I.e. at x=1 the volume of black carbon is $\approx 9 - 11$ % of the total semi-conducting compound. The unit on the y axis shows meter/siemens which is equivalent to Ωm. Figure and cited part of the caption obtained from El Hasnaoui et al. [110].

Many other studies have also measured this dependence, two of these can be seen below in Figure 3.4 [111] [112]. These have found similar results to those seen in Figure 3.3.

These also show the difference that different kinds of CB and polymer can have on both the percolation threshold and the resistivity before, and after, it.

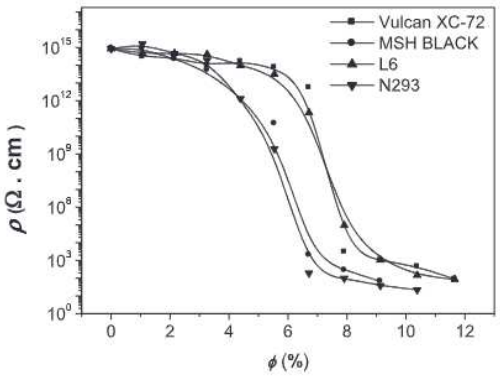

(a) Electrical resistivity of high density polyethylene compounds with four different types of CB. Figure taken from Liang and Yang [111].

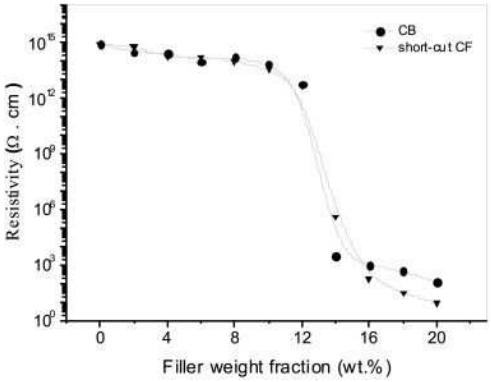

(b) Electrical resistivity of high density polyethylene compounds with either CB or carbon fibers. Figure taken from Liang and Yang [112].

Figure 3.4: Two further examples of previous studies done on the resistivity in semi-conducting compounds as functions of the concentration of CB.

In El Hasnaoui et al. [110], the temperature dependence of different CB concentrations was also studied. As seen below in Figure 3.5, the temperature dependence of resistivity strongly depends on the CB concentration. CB concentrations below the percolation threshold lead to a NTC while concentrations above it lead to a PTC.

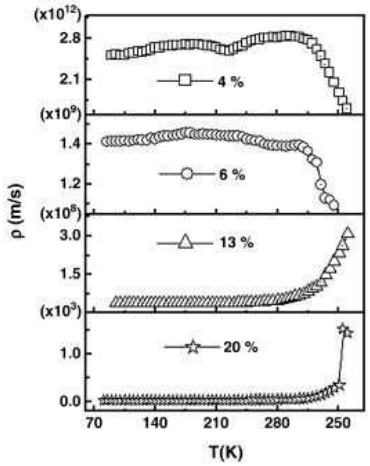

Figure 3.5: "Electrical resistivity as a function of temperature of the EBA/CB composites for four CB concentrations, two concentrations below the percolation threshold ϕ_c (ϕ= 4 % and ϕ = 6 %) and two concentrations above ϕ_c (ϕ = 13 % and ϕ= 20 %). Solid lines are drawn to guide the eyes." Note: The temperature written as 250 $°K$ should presumably be 350 $°K$. The unit on the y axis shows meter/siemens which is equivalent to Ωm. Figure and caption obtained from El Hasnaoui et al. [110].

At higher CB concentrations the materials behavior deviates strongly from regular semi-conducting materials. For those, the resistivity decreases with increasing temperatures as more and more electrons get thermally excited to the conduction layer. In contrast, the semi-conducting compound exhibits a strong exponential growth in resistivity with temperature.

Another study also examining the temperature dependence of the resistivity for varying CB concentrations is [113]. Some of its results can be seen below in Figure 3.6.

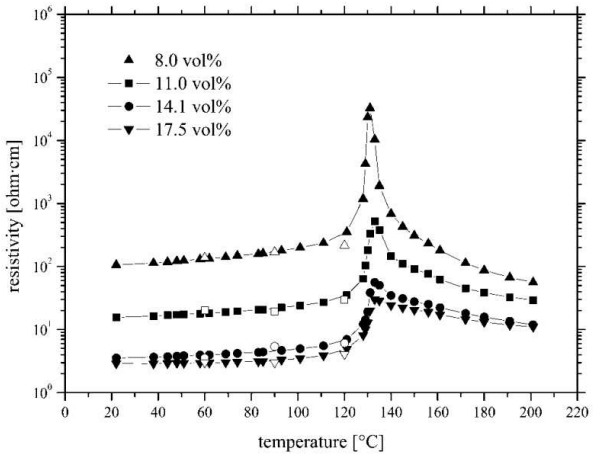

Figure 3.6: "Temperature dependence of the resistivity values for [...] HDPE–CB2 [...] composites filled with various CB amounts." Figure and caption taken from [113]. The caption was adjusted to remove discussions about other sub-figures.

Once again a strong increase in resistivity starts being seen as the compound reaches $\approx 100\ ^{\circ}C$, note the logarithmic y-axis. After peaking, a strong decrease in resistivity is seen, indicating the NTC region. There is also a clear difference when comparing the temperature at which the increase in resistivity starts at when comparing to Figure 3.5, making it clear that different compositions and types of materials can also adjust such parameters.

4 Methodology

This chapter describes the preparation of samples and how the measurements are conducted at sample level and product level.

4.1 Preparation of Sample

To create samples with easy access to the semi-conducting layer a standardized procedure in accordance with IEC standards 60840 § 12.4.9, 62067 § 12.4.9, 60811-401 along with the internal guidelines of the Material Technologies division at NKT was followed. The semi-conducting material is designed for transmitting voltages of 525 kV at a standard operating temperature of 70 $^{\circ}C$. The standard measuring temperature is, however, 90 $^{\circ}C$.

The sample preparation process started with a large length of cable, usually between one and two meters. The cable was then sawed into smaller pieces with the desired length of ≈ 200 mm. A picture of this starting point can be seen below in Figure 4.1

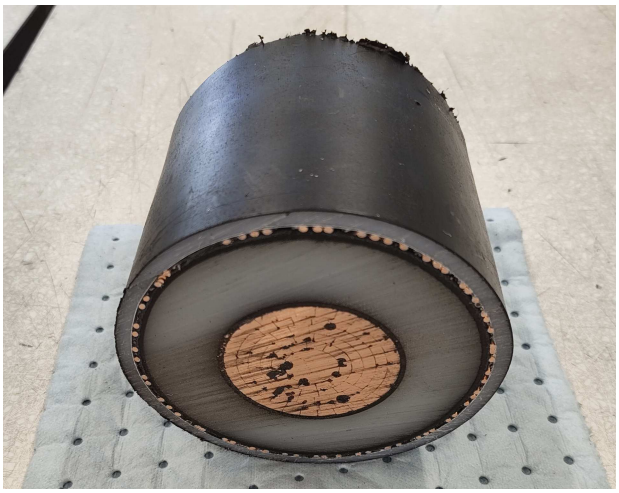

Figure 4.1: The starting point in the sample preparation process, a 200 mm piece of cable.

The outer sheaths of the samples were then cleaved and removed. Everything between the outer sheath and OSL, which to be clear are simply swelling bands and copper wires, were also removed. Below is a picture of the sample post cleaving with the protective sheath, copper wires, and swelling bands put to the side.

Figure 4.2: Picture showing the sample and everything that was removed during the first step of the sample preparation process. The sample, which is now ready for having electrodes applied if the OSL is to be studied, can be seen on the right. The removed swelling bands (top), protective sheath (right), and copper wires (middle) can also be seen.

At this point the sample consists of the four innermost layers, the conducting cable, ISL, insulation, and OSL. The samples were now ready for OSL-measurements but not ISL-measurements. To prepare an ISL-sample, an OSL-sample was cleaved down the middle and had its conductive cable removed. The swelling bands between the conducting cable and the ISL were also removed and the ISL was further cleaned to remove any remnants of the swelling bands. Every 200 mm section of cable could either yield one OSL sample or two ISL samples.

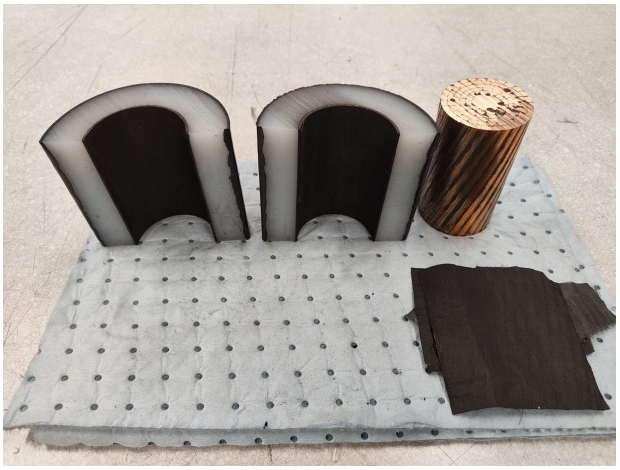

Figure 4.3: Picture showing the results of cleaving an OSL-sample with the purpose of creating ISL-samples. This yields two ISL samples (top left), the conductive core (top right), and swelling bands (bottom right).

With both ISL- and OSL-samples having been stripped down to their necessary parts the electrical contacts could now be added. Four $\approx 3-4$ mm thick lines of silver conductive paint, SCP, were painted at set distances from each other and acted as electrodes. Different types of SCP were used during the project with varying silver concentrations of $\approx 50-70$ %. The current was driven through the outermost electrodes which were placed 25 mm from the inner electrodes. The inner electrodes were used for voltage measurements and separated by a distance of 50 mm. A sketch of the samples seen below in Figure 4.4 and actual pictures of the finished samples in Figure 4.5.

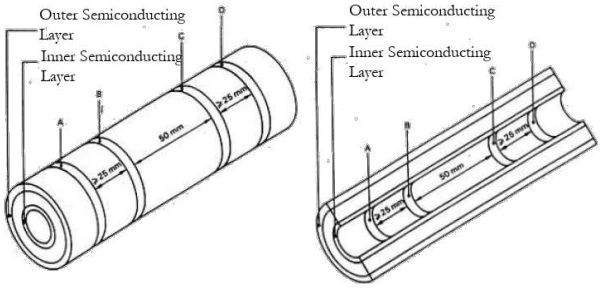

Figure 4.4: A sketch showing the finished samples before measurements. A sample for measuring the outer semiconducting layer can be seen on the left and for the inner layer on the right. Distances between the electrodes, A, B, C, and D, are also marked as 25 mm between A and B and C and D. The distance between B and C is 50 mm.

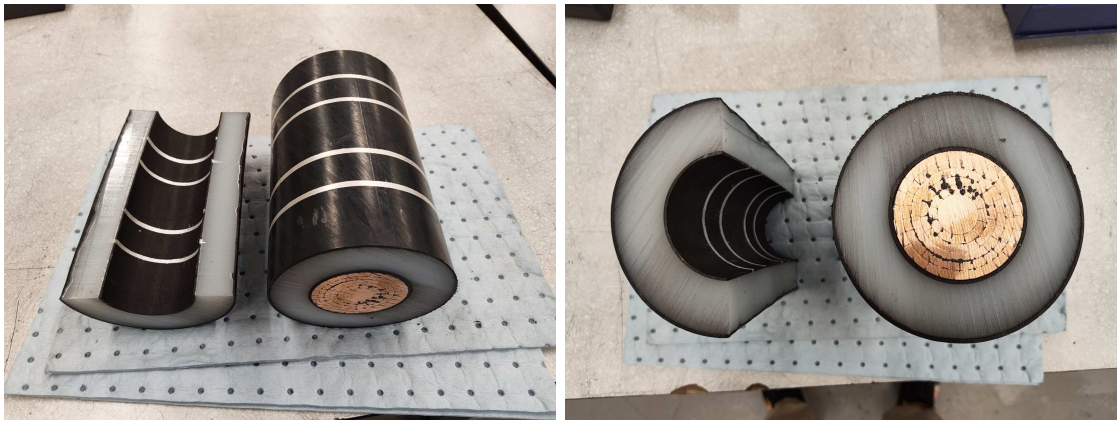

(a) **(b)**

Figure 4.5: Two perspectives of finished ISL and OSL samples with the same design as seen in the previous sketch. ISL samples are seen to the left in both pictures and OSL samples to the right.

As one can see in Figure 4.5, there is quite a big difference between the samples used to examine the ISL and OSL. The samples used for ISL measurements are half-cylinders

consisting of the ISL, insulation, and the OSL. The samples used for OSL measurements, on the other hand, are complete cylinders and consists of all the same parts, but with the addition of the conducting metal core. This means that there is a large mass difference between an ISL and OSL sample from the same cable. ISL samples weigh $\approx 0.85\ kg$ and OSL samples $\approx 7\ kg$. Furthermore, there is more stability against deformations for OSL samples compared to ISL samples due to the stabilizing presence of the core.

To measure the thickness and diameter of the samples two methods were used. Firstly, pictures of slices of cable were analyzed with software to give averages of the diameter and thickness. These measurements were also manually confirmed using a precise, digital caliper. Caliper measurements were performed on six different points on each side of the cable which were then averaged out. For samples were the software analysis was not available, only the caliper measurements were used.

4.2 Resistivity Measurements

The resistivity measurements themselves were also done in accordance with IEC standards 60840 § 12.4.9, 62067 § 12.4.9, 60811-401 along with the internal guidelines of the Material Technologies division.

After the sample had been prepared it was placed on an appropriate rig for measuring. These rigs had four probes that were placed on the electrodes. Three pictures of the rig itself, an ISL sample on the ISL side of the rig, and an OSL sample on the OSL side of the rig can be seen below in Figure 4.6.

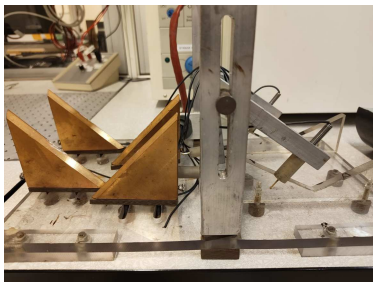

(a) The measuring rig used for all measurements except humidity measurements.

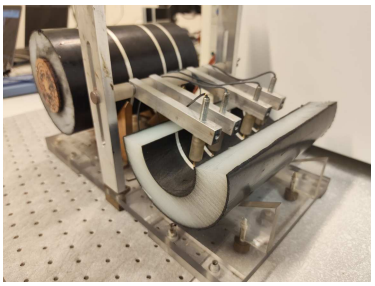

(b) An ISL sample on the ISL side of the measuring rig.

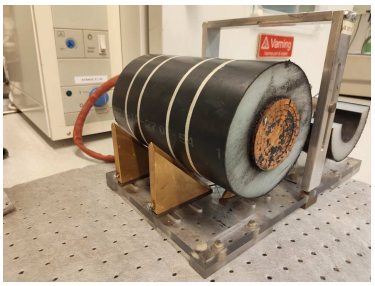

(c) An OSL sample on the OSL side of the measuring rig.

Figure 4.6

The probes were connected to a B2910BL Precision Source/Measure Unit [114] (SMU) which supplied pulses of current through the outer electrodes, measured the voltage over the two middle electrodes, found the resistance, and calculated the resistivity using the dimensions of the sample with Equation 3.3. Unless otherwise stated the injected current

was 10 nA and applied periodically every 45 seconds for a duration of 16 hours. The results were exported to a separate device where they were read and plotted using Python. Many different variables were studied to see the effect that they had on the resistivity over long measurements. These include:

- The effect of repeated measurements on one sample
- Using a constant measuring current or periodic (10 nA)
- Different temperatures (75, 90, 105 $°C$)
- Different types of semiconducting layers
- Cross-linked and non cross-linked materials (Samples for all other measurements were as a default cross-linked)
- Different shapes of OSL-samples
- Different humidities (10, 30, 50, 70, 90 %RH)

For each of different variables multiple different values were studied and each value studied multiple times to minimize the effect of potential errors. All samples started at room temperature before being inserted into the measuring location. Most measurements were performed in an oven set to 90 $°C$. Measurements were started right before this insertion, meaning that the first value comes from a room temperature sample.

4.2.1 Recreation of Introductory Results

For these measurements samples were procured from cables of the same type as the introductory measurements. They were not from the same length of cable but they were made in the same way. The samples were prepared using the previously described method, the same as for the original measurements. The measurements themselves were performed under the same circumstances as the old measurements, using the same temperature of 90 $°C$. Every 45 seconds a 10 nA current was driven through the sample and the resistance measured. The resistivity was calculated using the logged resistance.

4.2.2 Repeated Measurements

To examine whether measurements had some sort of ageing effect on the samples multiple measurements were performed on the same sample over a period of weeks. Before and after each measurement the thickness and diameter of the relevant semi-conducting layer was examined. The silver contacts were also optically confirmed to be intact. The intervals between measurements were large enough for the samples to rest and return to room temperature, ranging from a couple of days to more than a week. Two sets of measurements were performed using this method, one to examine the ISL and one for the OSL, each consisting of five separate data points. All of these measurements were performed at the standard measuring temperature of 90 $°C$. Every 45 seconds, for a duration of 16 hours,

a 10 nA current was driven through the sample to measure its resistance and calculate its resistivity.

4.2.3 Constant Injected Current

This was a quite simple measurement. A constant current, of the same magnitude as other measurements, of 10 nA driven through the sample for the entire measurement. The measurement was performed at the standard operating temperature of 90 $°C$. The resistance was measured and the resistivity calculated and logged every 45 seconds for 16 hours. A single measurement of this was done for both the ISL and OSL.

4.2.4 Temperature

These sets of measurements were the most extensive ones and constitute the largest single part of the project. For the study of the temperature's effect on resistivity, the measurement rig was put inside an oven set at varied temperatures. A current of 10 nA was supplied every 45 seconds for 16 hours, the resistance measured, and the resistivity subsequently calculated and logged. Measurements were performed at 75 $°C$, 90 $°C$, and 105 $°C$. For each of these temperature three measurements were performed. The temperature of the semi-conducting material was also measured and logged during the measurement. The method for measuring the temperature is described in section 4.3.

4.2.5 Different Types of Semi-Conducting Layers

To study the difference between different types of semi-conducting layers another model of cable with a different semi-conducting layer was compared to the temperature measurements in section 4.2.4. The samples were prepared and measured in the same way at the same temperatures (75, 90, 105 $°C$) as the aforementioned measurements. Measurements were performed every 45 seconds for a duration of 16 hours using a measuring current of 10 nA.

4.2.6 Non Cross-Linked Samples

Samples that had not yet been cross-linked along with the same type of samples but cross-linked were obtained from the NKT factory in Köln. The samples had the same semi-conducting material as all other samples and had already been prepared up until the electrode-painting step. Measurements were performed at 90 $°C$ using a measuring current of 10 nA every 45 seconds for a duration of 16 hours.

4.2.7 Different Shapes of OSL-Samples

To examine the effect that the shape and mass of OSL samples have on the results, an alternate design for OSL samples was prepared. A complete OSL sample was split down

the middle and had its conductor removed. This design is essentially an ISL sample but with the electrodes put on the outside. A picture showing the alternate design can be seen below in Figure 4.7.

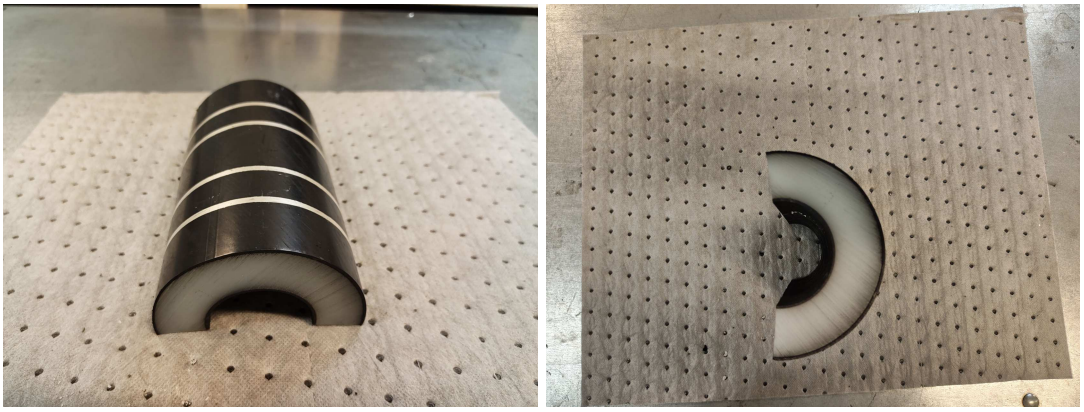

(a) **(b)**

Figure 4.7: Two perspectives of the alternative preparation for OSL samples.

The measurement itself was performed on the ISL side of the rig at the standard temperature of 90 $°C$ and with the standard measuring current, 10 nA, every 45 seconds for 16 hours.

4.2.8 Humidity

For humidity measurements a different rig employed. This rig was easier to use and provided better contact between the probes and electrodes. With it both the ISL and OSL could be measured simultaneously. Pictures of the rig with and without samples can be seen below in Figure 4.8.

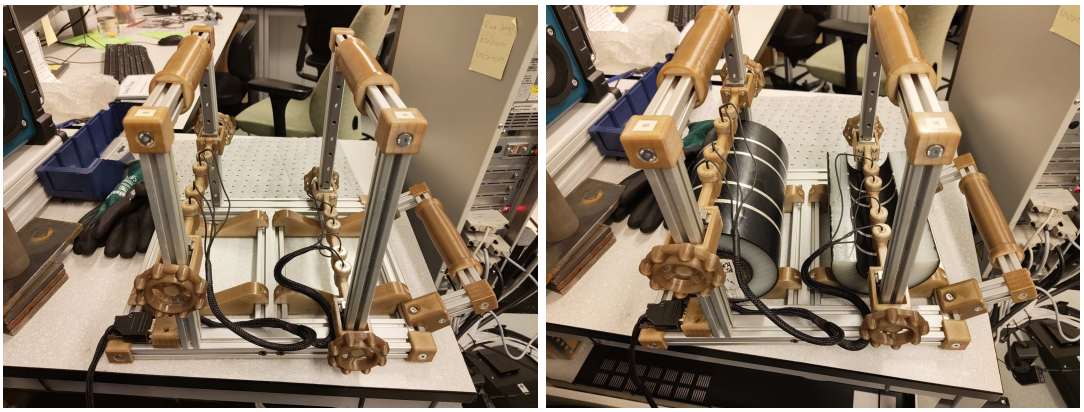

(a) **(b)**

Figure 4.8: Two pictures of the measuring rig used for humidity measurements, showing it both with and without samples.

The rig, with the samples, was put inside a climate chamber where humidity and temperature could be adjusted. The climate chamber itself was in a room with a relative humidity of 50 % and a temperature of 23 $°C$. A couple of hours before the start of the measurement the climate chamber was set at its desired temperature and humidity. A temperature of 80 $°C$ was always used while the relative humidity was varied. Room temperature samples were taken from outside the room with the climate chamber and immediately put onto the measuring rig. The rig was then fastened and the measurements started. The same type of SMU was used as in the temperature measurement and the same measuring current of 10 nA was used.

4.3 Temperature Measurements

As many of the tests are performed at elevated temperatures it is also interesting to examine the duration it takes for samples to reach the temperature of their environment. For this purpose a K-type thermocouple wire was used. A small hole with a diameter of ≈ 2 mm, about the same diameter as the wire, was drilled into the sample approximately 2 cm from the outermost electrode. The hole was drilled diagonally into the semi-conducting layer such that it is roughly in the middle of the layer, about 1 mm deep. The thermocouple wire was inserted into the cavity far enough into it such that only the brown protective jacket can be seen. A piece of tape is then applied on the wire to keep it in place without covering the hole. Three pictures showing the main steps for this can be seen below in Figure 4.9.

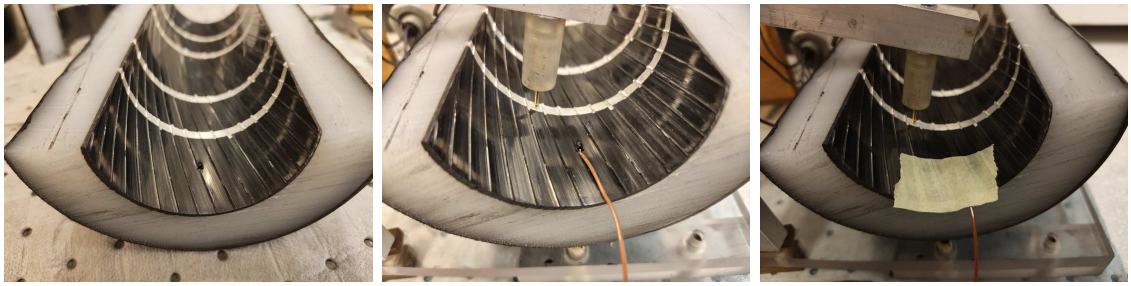

(a) **(b)** **(c)**

Figure 4.9: Three pictures showing the process of inserting the K-type thermocouple wire into an ISL sample.

This process was developed by the author of this thesis and was not based on any pre-established standards. The method was, however, discussed with others and a couple of different things were considered, the main ones being the following:

- To not affect the measurements. This was done by placing the wire outside of the outermost electrode.

- To get a temperature that reasonably represented the semi-conducting layer as a bulk. This was done by placing the wire in the middle of the layer and not too close to any edge.
- To make sure that the measured value actually represented the temperature of the semi-conducting layer and not the air around it. This was done by drilling the hole at an angle and making it such that its diameter was the same as the wire. This made sure that airflow between the probe and the outside air was minimal.

Before each measurement the thermocouple wire was also tested at a known temperature to make sure that the measured values were reliable.

4.4 Optical and Chemical Characterization

To get a better understanding of the surface of the samples and any possible contaminants a scanning electron microscope (SEM), equipped with energy dispersive X-ray spectroscopy (EDS) was employed. Understanding the topology of the surface along with types of contaminants can be very important when it comes to contact resistance [115][116][117].

For the SEM and EDS analysis separate samples were created. These were simply small pieces cut from the same cables as the normal samples and consisted of either a part of the ISL or OSL along with some insulation. These samples were approximately 7 mm thick. They were then cleaned and contacts were created on parts of the samples.

5 Results and Discussion

This chapter describes the results obtained from all the types of measurements described in the previous chapter. The exact methodologies used to prepare and measure the samples are described in chapter 4. Some brief summaries of the methodology will, however, still be provided at the beginning of each section. Something that goes for all measurements is that the samples started at room temperature before being inserted into the measuring area. This also means that the start of the measurement show the transition between room temperature and the measuring conditions.

Before looking at the results, it can be important to keep in mind some differences between individual samples and between ISL and OSL samples. Each measurement is performed on a new sample, all of which naturally vary slightly. Discrepancies between measurements that are expected to look the same can therefore occur simply due to these inherent variations. While the ISL and OSL consist of the same material, they differ in how they are applied to the cable during production. ISL and OSL samples also differ in shape and size. Differences between ISL and OSL results do therefore not indicate some difference in material property, but rather come from differences in production and sample preparation.

5.1 Recreation of Introductory Results

As a start, the results that initiated the thesis are recreated. These recreations are plotted together with the original results below in Figure 5.1. Note the logarithmic y-axis.

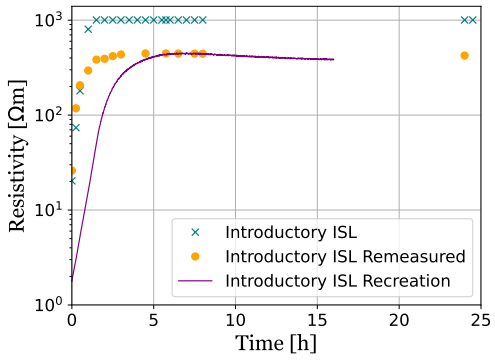

(a) The recreation of the introductory ISL results plotted together with the introductory measurement and its re-measurement.

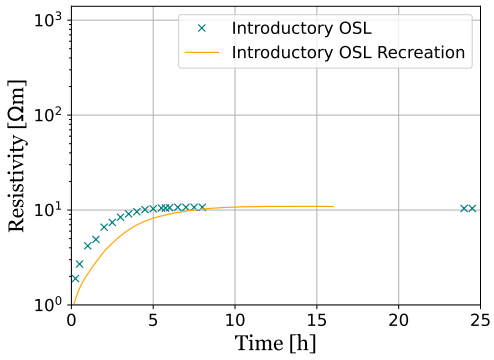

(b) The recreation of the introductory OSL result plotted together with the introductory measurement.

Figure 5.1: Recreations of the introductory results that initiated this thesis plotted together with their corresponding introductory measurements.

In general the recreations seem quite similar to the original ones but with one clear discrepancy: the time it takes to reach the peak. For both the ISL and OSL it takes longer for the recreation to reach its peak compared to the original. This effect is more noticeable for the ISL than OSL, but is clearly present in both. Concerning the ISL sample the recreation takes $\approx 3\ h$ longer to reach its peak while the OSL sample takes an additional hour to reach its peak. The resistivity values that the recreations end up at seem consistent with the introductory measurements.

There are a couple of reasons that could explain the discrepancies between the two results. A minor difference is regarding when the measurements were initiated. In the original results, the sample was put into the oven before the first data point. In contrast, the measurements for this thesis were started while the sample was outside the oven at room temperature before quickly being inserted into the oven. This should constitute a difference of at most a couple of minutes and does not seem like a reasonable explanation for the differences seen in Figure 5.1.

Another possible explanation would be a difference in the samples themselves. The recreation samples were taken from the same type of cable but not from the same length of cable. This means that there could be differences between the cables simply resulting from them being created in different ways. There was also a significant divergence when it comes to the diameter, D, and thickness, t between introductory and recreation measurements. These are detailed below in Table 5.1.

Table 5.1: The thickness and diameter of samples for both the introductory measurements and their recreations.

	$D\ [mm]$	$t\ [mm]$
Introductory ISL	68	2.2
Recreation ISL	61	1.4
Introductory OSL	124	2.0
Recreation OSL	112	1.4

The differences in D and t should only affect the results by a relatively small factor judging from Equation 3.3 and once again do not seem to be a satisfactory explanation of why the samples take longer to reach their peak resistivity. A final possible explanation for these differences would be changes to the methodology and equipment. The introductory measurements were performed three years prior to the creation of the thesis and since then SCP, SMU, and measuring rig have all been changed. Nonetheless, the recreations were still successful as they share the general characteristics and approximate resistivity values as the introductory measurements,

5.2 Repeated Measurements on One Sample

The two sets of repeated measurements on ISL and OSL samples can be seen below in Figures 5.2a and 5.2b respectively. The legend and indexes indicate the dates that the measurements were performed in the format YYMMDD.

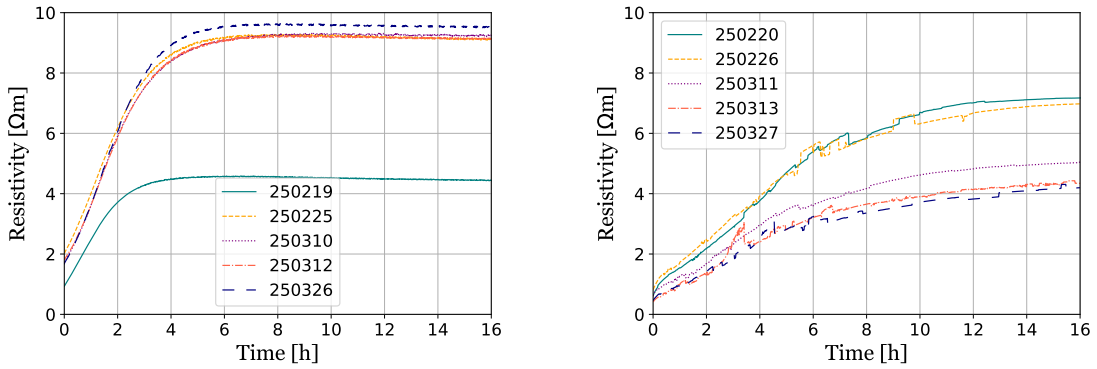

(a) **(b)**

Figure 5.2: Two graphs, each showing multiple measurements of the same sample performed at different times for one ISL sample (a) and one OSL sample (b). The legends indicate the dates (YYMMDD) that the measurements were started.

Here the first measurement, 250219, has about half of the resistivity compared to all other measurements. Although this would not be impossible, it is also to be noted that the thickness of the semi-conducting layer was registered as 1.01 mm, less than half of the thickness after the first measurement. It is somewhat likely that this was simply a typo and that the thickness in actuality was 2.01 mm. This second thickness also aligns better with measurements on similar pieces. The same measurement but adjusted for this can be seen below in Figure 5.3.

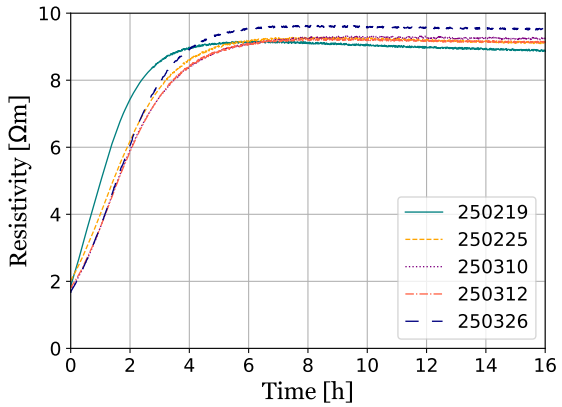

Figure 5.3: Adjusted version of Figure 5.2a where the first measurement, 250219, has been multiplied with a factor of two to make up for what could have been a typing error.

It is, however, also possible that all measurements except the first one had their thicknesses incorrectly inputted. Both the OSL plot in Figure 5.2b and many of the plots that will be discussed in the following sections that were performed at the same temperature ended up close to 5 Ωm, the same as the 250219 measurement. The truth could naturally also be somewhere in the middle with the initial thickness being written as too small and all of the following as too large. Regardless of the quality of the results, these measurements act as a clear example that the method for measuring thickness was less than ideal, leading to unnecessary uncertainties.

Looking at Figure 5.2b a consistent decrease in resistivity for each measurement can be seen. This change is not radical but it indicates that there is some aging, that results in a decrease of resistivity.

The diameter, D, and thickness, t, was also measured before and after each measurement. A table of D and t before and after the initial measurement can be seen below in Table 5.2. D and t were remeasured after every subsequent measurement but always tended back towards the values seen after the first measurement which is why only those are shown below.

Table 5.2: The diameter and thickness of samples pre- and post-measurement. The post measurement values were obtained after the sample had cooled down, i.e. these values do not come as a consequence of thermal expansion of a hot object.

	D **pre [mm]**	t **pre [mm]**	D **post [mm]**	t **post [mm]**
ISL Sample 1	67	2.0	62	2.10
OSL Sample 1	124	2.1	125	1.95
ISL Sample 2	66	1.65	62	1.75
OSL Sample 2	121	1.35	122	1.35

In general the results stay somewhat consistent throughout repeated measurements, keeping the same characteristics over time but with slightly adjusted values of resistivity. Part of the reason for differences in resistivity come from the changes in D and t shown in Table 5.2. For ISL samples a decrease in D and an increase in t was seen while for OSL samples the opposite of an increase in D and decrease in t was noted. All measurements also start at approximately the same value indicating that the samples return to their initial states after cooling down post measurement.

5.3 Constant Measuring Current

A single measurement was conducted for both an ISL and an OSL sample using the constant power mode on the SMU. This meant that the measuring current of 10 nA was continuously driven through the sample. Measurements were still only recorded every 45 seconds. The results from these measurements are presented below in Figure 5.4.

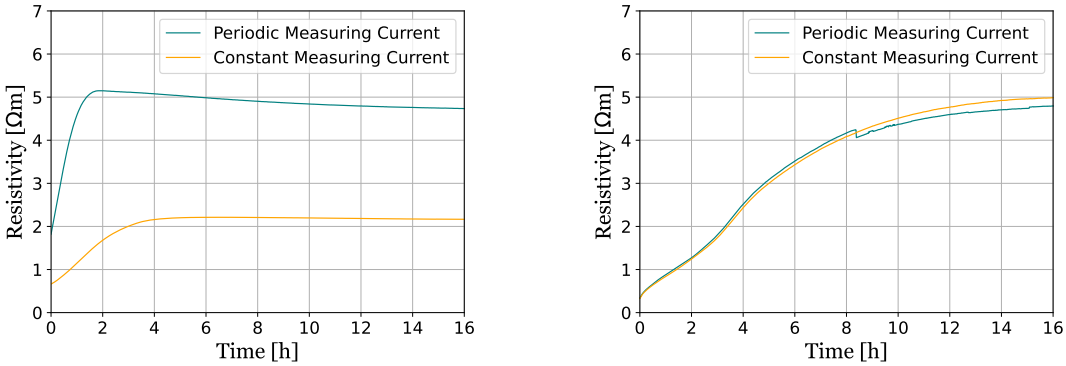

(a) **(b)**

Figure 5.4: Graphs showing the difference in resistivity between having a periodically or constantly applied measuring voltage for ISL (a) and OSL (b).

As can be seen, there does not seem to be an especially large difference between plots with a constant measuring current and periodically driven measuring current. The OSL curves are essentially identical while there is more of a difference between the ISL curves. The ISL curves are, unfortunately, not that reliable due to mistakes made in the methodology. The OSL measurements were performed in the same period of time on the same batch of cable while the ISL measurements were performed months apart and with samples from different cable batches. Due to a lack of available cable pieces at the time the constant measuring current measurement for the ISL was also performed on a sample that had been previously been used on a humidity measurement which could further have affected results. Due to a lack of time no backup measurements were performed which further increases the

uncertainty of the ISL measurement. The much more reliable OSL result shows how a constant measuring current does not affect results.

It is not necessarily an unexpected that a constantly driven measuring current would not affect the results significantly. It was still interesting to study it to see whether the semiconducting material would act as a capacitor, that would provide possibility to measure and assess permittivity apart from resistivity, with the polymer acting as a dielectric between the conductive carbon. If this was the case and since DC current was used for measurements, the current would likely stop flowing as the capacitors charged, significantly increasing the resistivity. This also nicely aligns with previous studies on CB polymer compounds being quite bad capacitors [118].

5.4 Temperature Effects

Temperature measurements were performed at three different temperature points: 75, 90, 105 $°C$. The results from these measurements are presented in Figure 5.5.

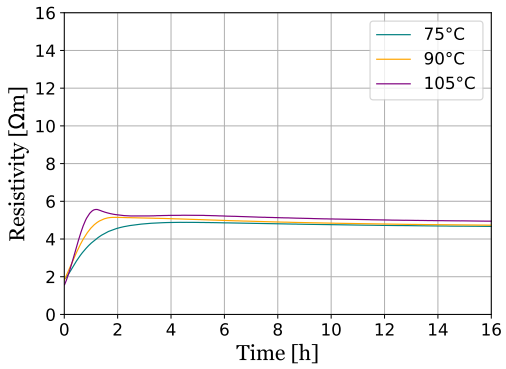

(a) The resistivity of ISL samples as a function of time for three different temperatures, 75, 90, and 105 $°C$.

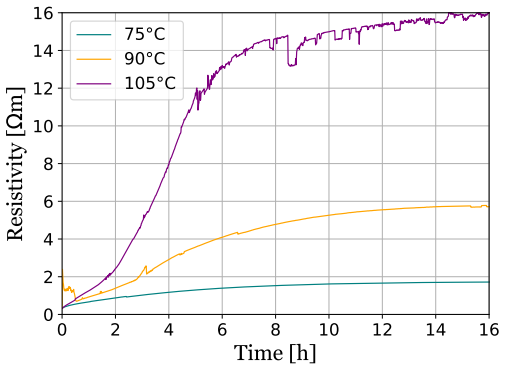

(b) The resistivity of OSL samples as a function of time for three different temperatures, 75, 90, and 105 $°C$.

Figure 5.5: Two graphs showing the resistivity of ISL and OSL samples as a function of time for three different temperatures, 75, 90, and 105 $°C$.

It is clear that ISL and OSL results have very different characteristics. ISL samples reach their peak resistivity after about two hours, after which the resistivity slowly starts dropping, while the resistivity in OSL samples keep on increasing even after 16 hours. The resistivity difference between different temperatures in OSL samples are also much larger than in ISL samples where all results tend toward the same value.

That the ISL results all reach the same value indicate that the ISL has a superior temperature resistance when compared to the OSL. This is desirable as the ISL faces higher

temperatures during normal use than the OSL.

Looking closer at Figure 5.5a, there is another detail separating it from the OSL results. At the beginning of the measurement, roughly one to two hours in, the resistivity peaks. This peak becomes more distinct at higher temperatures, being quite obvious at 105 $°C$, barely noticeable at 90 $°C$, and seemingly non-existent at 75 $°C$. This peak could potentially come as a result of the NTC seen at larger temperatures for the semi-conducting compound. If this was the case, something similar should probably be seen on OSL measurements as well. This is, however, not the case. Another explanation for the peak could be the thermal expansion of the rest the sample. As the insulation layer of an ISL sample heats up and expands, it partly crumples up, decreasing D and slightly increasing t, in turn decreasing ρ. This decrease had a magnitude of approximately 6.5 %.

A detail that needs to be disclosed is that the ISL and OSL samples came from different cables. The materials that composed the cables were still the same and the samples were prepared in the same way. It was determined that this would not affect the results. The main difference between the cables was a slight difference in size. This difference should be easily ignored as ISL and OSL samples always have different sizes and the dimensions of the sample are adjusted for in the resistivity calculation.

The simplest explanation for differences in the results comes from the widely different masses of the samples. OSL samples have almost 10 times the mass of ISL samples ($\approx 0.85kg$ for ISL and $\approx 7kg$ for OSL). It seems reasonable that this would lead to the semi-conducting layers and the rest of the cable heating up at different paces. To examine this, the temperature change over time for inner and outer semi-conducting layers were plotted and can be seen below in Figure 5.6.

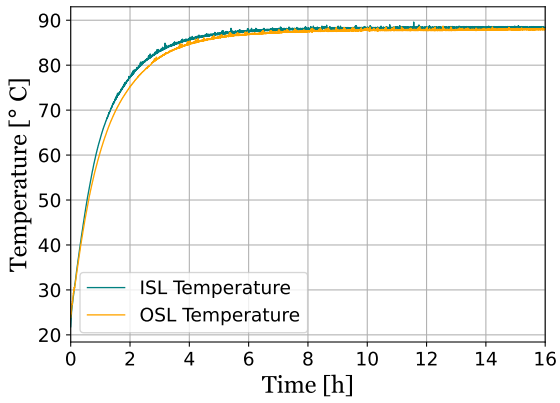

Figure 5.6: Graph showing the change in temperature for the inner and outer semi-conducting layers as a function of time. The sensor is placed inside the middle of the semi-conducting layer, roughly 1 mm deep.

Although the ISL heats up slightly faster, this difference is minimal and can not explain the stark difference between the results in Figure 5.5. This does not mean that ISL and OSL samples react the same to being heated up. The results in Figure 5.6 only show the temperature in the middle of the semi-conducting layers and not in other parts such as the insulating layer. The insulating layer, constituting the largest fraction of a sample and being a thermal insulator, heats up very slowly. This means that the thermal expansion of this layer will take much longer than the roughly two hours it takes for the semi-conducting layer to heat up.

As the insulating layer expands, it changes both the diameter and thickness of the semi-conducting layers. This is where a clear difference between ISL and OSL samples can be seen. Without the stabilization of the conducting core, ISL samples partly collapse in on themselves, crumpling up like a spider's legs post mortem, decreasing the diameter. The reduction in diameter of the sample also increases the thickness of the semi-conducting layer. Examples of these changes after a sample had cooled down following a measurement can be seen in Table 5.2 but are summarized as follows: on average ISL samples had their diameter reduced by $\approx 4.5\ mm$ (≈ 6.5 %) and their thickness increased by $\approx 0.1\ mm$ (≈ 5 %). OSL samples, on the other hand had their diameters increased by $\approx 1\ mm$ (≈ 1 %) and their thickness decreased by $\approx 0.1\ mm$ (≈ 5 %).

This offers some explanation to why the resistivity would continually increase/decrease for OSL and ISL samples respectively and could quite nicely describe Figure 5.5a. Figure 5.5b is a bit trickier as the long term change in resistivity is larger compared to Figure 5.5a, but it seems likely that this change just comes as a result of a combination of all the aforementioned reasons.

Focusing in on only the transient region, where most of the changes in resistivity happen is also interesting. As seen in Figure 5.6 it takes roughly 6-8 hours for the semi-conducting material to reach its equilibrium value.

Plotting the resistivity as a function of time together with the temperature as a function of time can give a more detailed idea about the relationship between temperature and resistivity.

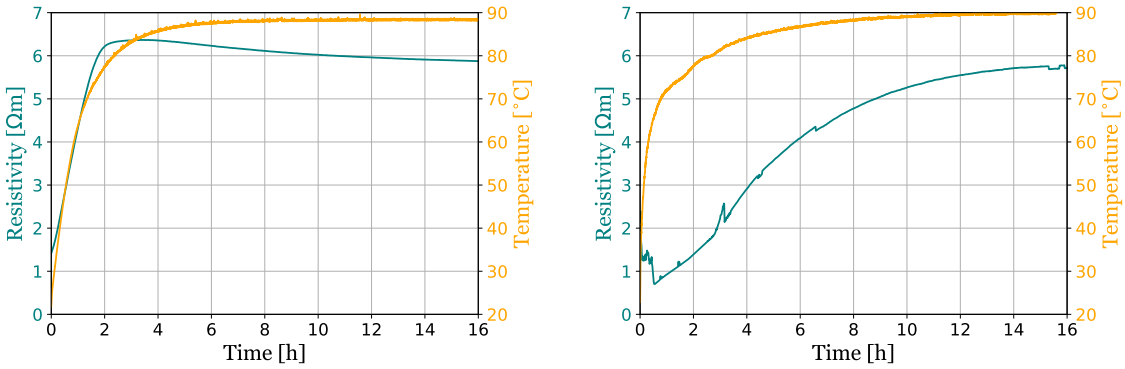

(a) The resistivity of an ISL sample measured at 90 $°C$ together with its corresponding temperature as a function of time.

(b) The resistivity of an OSL sample measured at 90 $°C$ together with its corresponding temperature as a function of time.

Figure 5.7: Two graphs showing the resistivity of an ISL and OSL sample plotted together with its corresponding temperature curve.

For the ISL, the resistivity follows the temperature quite closely as a start but starts to decrease as it reaches 90 $°C$. The resistivity of the OSL, in contrast, is not really affected by temperature increases in the beginning of the measurement before quickly increasing as the temperature approaches 90 $°C$. Accurately measuring temperature is difficult, and the depth at which the probe is placed matters greatly. It is probable that the probe for for the ISL sample was placed at a deeper depth than the probe in the OSL sample which explains why it takes longer to heat up. This difficulty will lead to some errors that will also propagate through the following results.

To get a better understanding of the plots in Figure 5.7 they are recreated showing resistivity as a function of temperature which can be seen below in Figure 5.8.

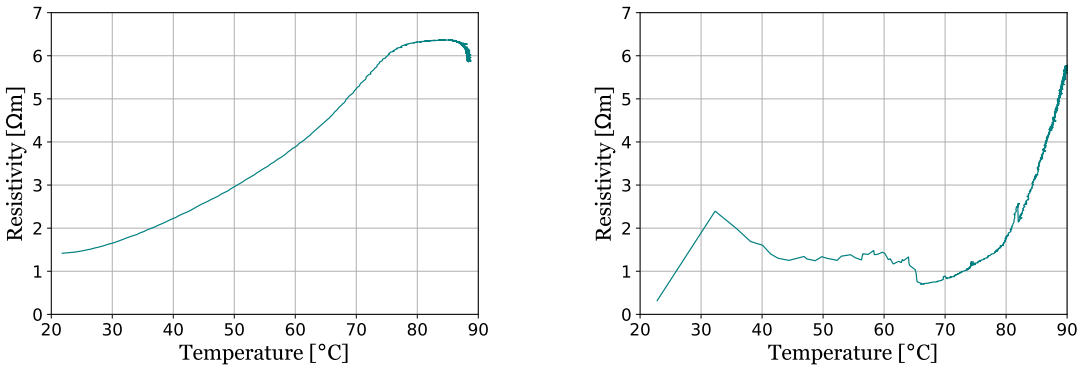

(a) Resistivity plotted as a function of temperature for the ISL sample in Figure 5.7a.

(b) Resistivity plotted as a function of temperature for the OSL sample in Figure 5.7b.

Figure 5.8: The resistivity as a function of temperature for the results in Figure 5.7.

This further emphasizes the weak exponential increase in resistivity for the ISL results and the stronger exponential increase for the OSL result. Although these results are interesting, they also suffer from a somewhat scuffed x-axis since most data points exist at higher temperatures. This explains why the small jump in resistivity at the beginning of Figure 5.7b takes up much more space in Figure 5.8b. Therefore, the points at higher temperatures are also more reliable.

The exponential temperature dependence of the resistivity aligns with a tunneling based conduction method, supported by previous studies such as El Hasnaoui et al. [110], seen in Figure 3.5.

To get a better understanding of this exponential relationship the heat-resistivity coefficient, α, can be examined. Equation 3.5 can be rewritten to give α.

$$\alpha = \frac{\frac{R}{R_0} - 1}{T - T_0} \tag{5.1}$$

Calculating α for every temperature and plotting it as a function of temperature shows how much the resistivity is affected by temperature at different points. Two graphs showing α as a function of temperature and its corresponding resistivity as a function of temperature graph can be seen below in Figure 5.9.

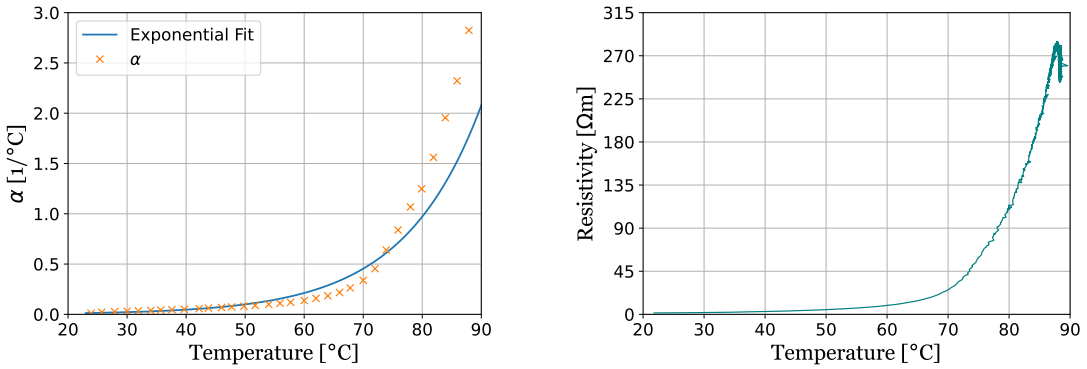

(a) α plotted as a function of temperature together with an exponential fit.

(b) The corresponding resistivity vs temperature measurement.

Figure 5.9

As expected there is a strong increase in α towards higher temperatures with α at 90 $°C$ being roughly 280 times larger than α at 23 $°C$, $\alpha(90) = 2.8$ and $\alpha(23) = 0.01$. To clarify, this means that the resistance grows at 280 times the speed at 90 $°C$ compared to 23 $°C$. These values can starkly contrast each other for different samples, with some samples only seeing a change in α by a factor of 5, but the same general trend can nevertheless always be seen. In Figure 5.9a an exponential fit has been applied although it does not fit particularly well. From the theory discussed in section 3.3.2 two main explanations are given for how resistivity changes over temperature: an exponential increase in resistivity from the CB agglomerates getting spread out and an exponential decrease resulting from the rise in electron energy. It therefore seems likely that α would also follow an exponential curve which is why an exponential fit was chosen. Other fits, namely different polynomials were also used but did not yield any better results. By plotting α and the fit with a logarithmic y-axis it is easier to examine how α diverges from an exponential behavior.

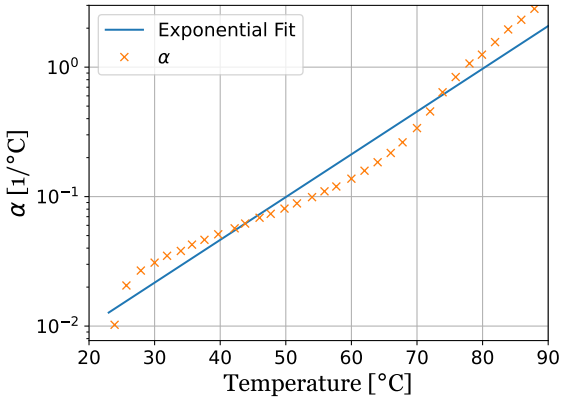

Figure 5.10: Figure 5.9a but plotted with a logarithmic y-axis.

Although the aforementioned explanations given in section 3.3.2 are reasonable and widely accepted [64][97][98][119] they do paint a slightly misleading picture. The problem comes from the fact that increases in resistivity due to widening gaps between CB agglomerates has a complicated relationship with temperature. An increase in temperature does not directly correlate to an increase in distance between CB agglomerates, in fact the average distance remains the same, but rather to an increased probability that larger gaps form. Looking at it another way, T is not necessarily proportional to w. There is still a dependence of w on T but an increase of X $^{\circ}C$ does not necessarily correlate to an increased w of $C \cdot X$ where C is some coefficient, constant or otherwise.

α goes through three distinct regions in Figure 5.10. Between $\approx 20 - 30$ $^{\circ}C$ α increases strongly as equilibrium conditions are broken, faster than the exponential fitting. Between $\approx 30 - 70$ $^{\circ}C$ α still increases but at a slower pace before reaching another strong increase again above 70 $^{\circ}C$. This last point, at 70 $^{\circ}C$ is approximately the glass transition temperature of the polymer where more radical changes in structure are to be expected. The general trend, however, remains the same, with increasing temperatures increasing both α and ρ.

All of this to say that the temperature dependence of resistivity is complex. There are also large differences in values of α between different samples, even with the same type of semi-conducting material. The same general behavior of α increasing with T is still always seen. Two examples showing other α behaviors are shown below in Figure 5.11.

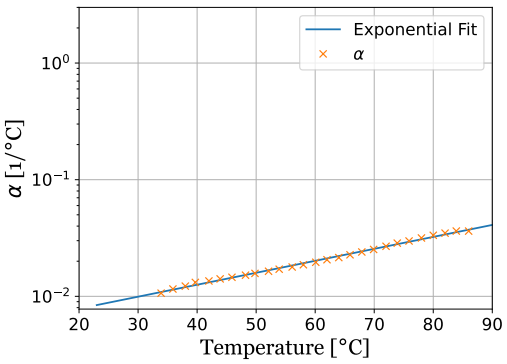

(a) α for the constant measuring current plot in Figure 5.4a, plotted with a logarithmic y-axis.

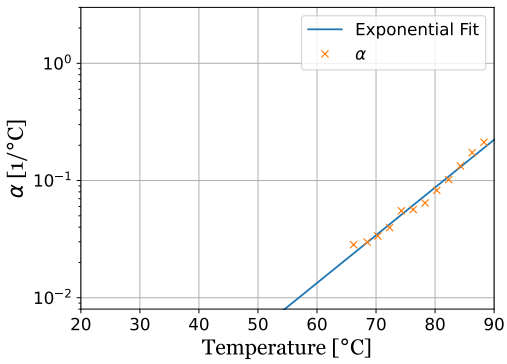

(b) α for the OSL measurement in Figure 5.7b, plotted with a logarithmic y-axis.

Figure 5.11: Examples of α for two other measurements. Showing the large differences in α between different samples.

5.5 Different Types of Semi-Conducting Layers

For this measurement two types of semi-conducting materials are compared "Type 1" and "Type 2". Type 1, is the same material seen in all other measurements.

Measurements on Type 2 were performed in the same way as the measurements for section 5.4 and are compared to the results of that section. To be clear, the Type 1 measurements are the same ones seen in Figure 5.5. Measurements of both Type 1 and 2 can be seen plotted together in Figure 5.12.

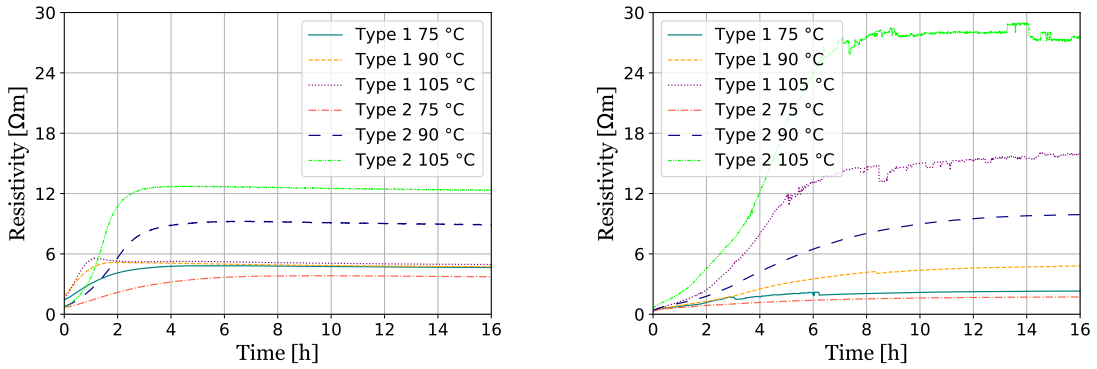

Figure 5.12: The resistivity values of ISL samples (a) and OSL samples (b) with two different types of semi-conducting materials as a function of time at three different temperatures, 75, 90, and 105 $°C$. The Type 1 measurements are the same as the results in Figure 5.5.

In every single case the Type 2 material has a higher resistivity than the corresponding Type 1 material measurement. In the ISL measurements, seen in Figure 5.12a, the distinctive peak is missing from the higher temperature measurements. The Type 2 measurements also distinctly take a longer time to peak compared to their corresponding Type 1 measurements. It is a bit harder to tell from the OSL measurements in Figure 5.12b but the same increase in time seems to be present there as well. Even though these differences are not huge, it is still clear that the semi-conducting material can be adjusted to adapt for different circumstances.

5.6 Cross-Linking

Samples from cables before and after cross-linking were obtained from the NKT factory in Köln. These had the same semi-conducting material as all other samples and were

measured at 90 $°C$ every 45 seconds for 16 hours. The results from these measurements can be seen below in Figure 5.13.

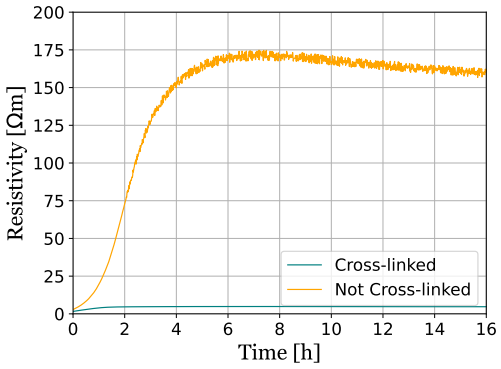

(a) The resistivity of a cross-linked and non cross-linked ISL sample.

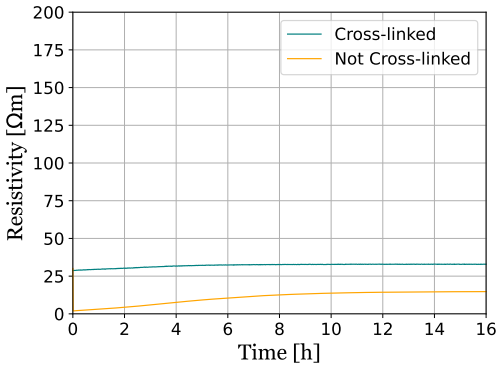

(b) The resistivity of a cross-linked and non cross-linked OSL sample.

Figure 5.13

The ISL results align quite nicely with expectations, with the temperature having a much larger effect on the non cross-linked sample compared to the cross-linked one. As previously discussed an increase in temperature leads to an increase in resistivity due to the breaking up of conductive pathways. As the non cross-linked polymer has a much lower temperature resistance this effect gets amplified for non cross-linked results.

The OSL results are confusing. The cross-linked sample starts at a high resistivity of > 25 Ωm and then barely change over the entire period, reaching a peak resistivity of ≈ 33 Ωm. A closer look at all OSL measurements can be seen in Figure 5.14.

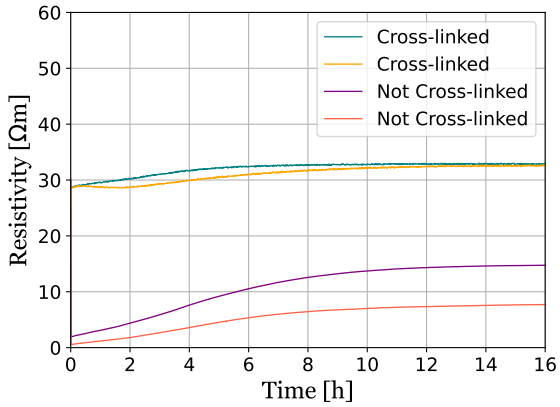

Figure 5.14: A closer look at all OSL results for cross-linked and non cross-linked samples.

The same weird behavior for the cross-linked samples was seen in both measurements, which were performed on two separate samples. The results from the non cross-linked samples look very similar to normal OSL results performed at 90 $°C$, although possibly with slightly higher values of resistivity. Explaining these results from a physics standpoint is difficult and it seems more likely that there was something wrong with the samples themselves. The results were expected to follow the behavior seen in Figure 5.13a with cross-linked results being expected to look like standard OSL measurements at 90 $°C$, while the non cross-linked ones being expected to have the same characteristics, but with exaggerated values as the temperature increases,

5.7 Alternate OSL Design

For this measurement an alternate OSL design was prepared, essentially just being a normal ISL sample but with the contacts on the outside. It was also measured on the ISL side of the rig at 90 $°C$. Below, in Figure 5.15, the results from the alternate OSL preparation is plotted together with ISL and OSL samples at the same temperature.

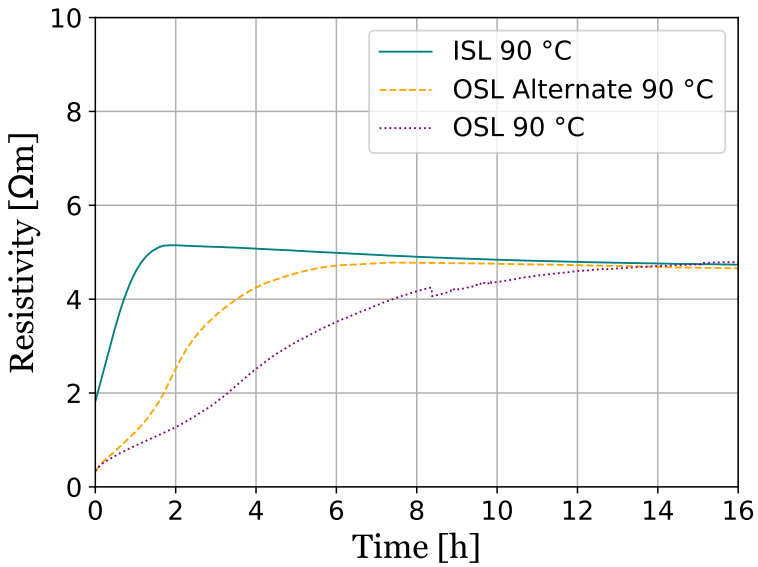

Figure 5.15: The resistivity of the alternate OSL design at 90 $°C$ plotted together with normal ISL and OSL samples at the same temperature.

Although all three measurements end up at approximately the same resistivity they all take different ways to get there. As can also be seen in previous measurements, it takes longer for OSL samples to reach their steady state than ISL samples with the alternate

OSL design landing somewhere in the middle. As expected, the alternate OSL sample acts as something in between an ISL and OSL sample, which it essentially is.

A possible explanation for the differences seen could have to do with the amount of semi-conducting material on each sample. The alternate OSL design has half the amount of semi-conducting material as a normal OSL sample but still significantly more than an ISL sample. It is possible that the semi-conducting compound heats up slower when there is more of it. This should in turn increase the time it takes for the resistivity to peak. This does not really align with the results in section 5.4, but a potential problem with those temperature measurements is that they only measured the temperature at a single point. It is possible that they do not give a good idea of the material as a whole and that the speed at which it heats up indeed depends on the size of the sample.

5.8 Humidity Effects

To examine the effect that humidity has on the resistivity, a climate chamber with adjustable temperature and humidity was employed. All measurements were performed at a temperature of 80 $°C$.

Measurements for ISL and OSL respectively at five different values of relative humidity can be seen below in Figure 5.16.

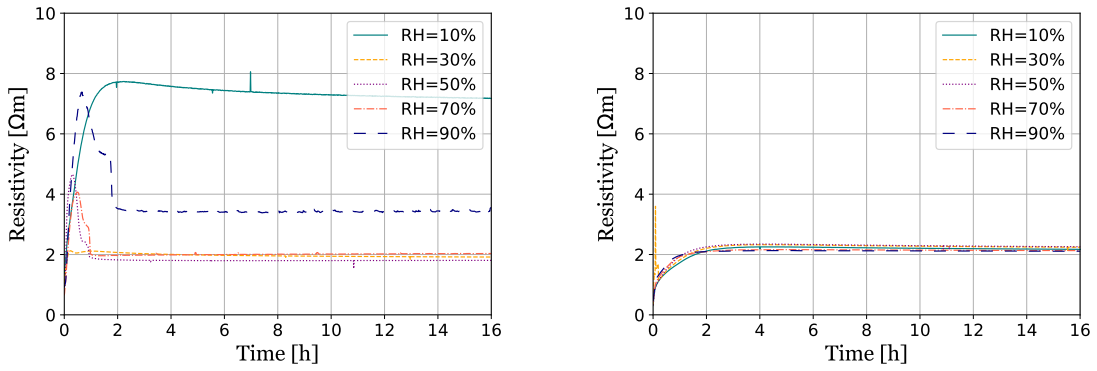

(a) The resistivity of ISL samples as a function of time at five different values of relative humidity: 10 %, 30 %, 50 %, 70 %, and 90 %.

(b) The resistivity of OSL samples as a function of time at five different values of relative humidity: 10 %, 30 %, 50 %, 70 %, and 90 %.

Figure 5.16

It is important to note that most, if not all, of the relative humidity values will not be reached under normal usage. Not only does the protective jacket block any external moisture but the swelling bands are also extremely at efficient at absorbing any moisture

that could have gotten past the jacket. The ISL is even less likely to be affected by any humidity as moisture would have to get past the OSL, insulation layer, and another layer of swelling bands to affect it. The results are nonetheless presented and discussed.

The ISL measurements in Figure 5.16a are, in general, quite different from the regular temperature measurements. A strong increase in resistivity is still seen at the beginning before a similarly quick decrease after only $\approx$ 30 minutes. There is then a plateau, the size/width of which increases with increasing values of relative humidity before another quick decrease in resistivity which then finally leads to the steady state. There is one clear outlier, the RH=10 % measurement, which looks almost identical to regular temperature measurements. This can just be explained by the humidity not being high enough to affect results. All of the other measurements, with the exception of the 90 % measurement end up at the same resistivity of $\approx 2\ \Omega m$. It seems unlikely that the 90 % result should differ from the other measurements and this difference can probably be explained by measuring errors.

The OSL measurements at all values of relative humility are essentially identical and all end up at the same resistivity. This is the same value that most of the ISL measurements also ended up at. A reasonable explanation for this would be that enough moisture formed on the samples such that the water on the surface was actually measured and not only the semi-conducting material itself. That all of the results reach their steady state values as quickly as they do further support the idea that the water on the surface is what is actually being measured.

5.9 Optical and Chemical Characterization

SEM imaging was performed on both ISL and OSL surfaces to examine the amount and types of contaminants. The contaminants where then analyzed using EDS to understand their origins. SEM images of parts of ISL and OSL samples can be seen below in Figure 5.17.

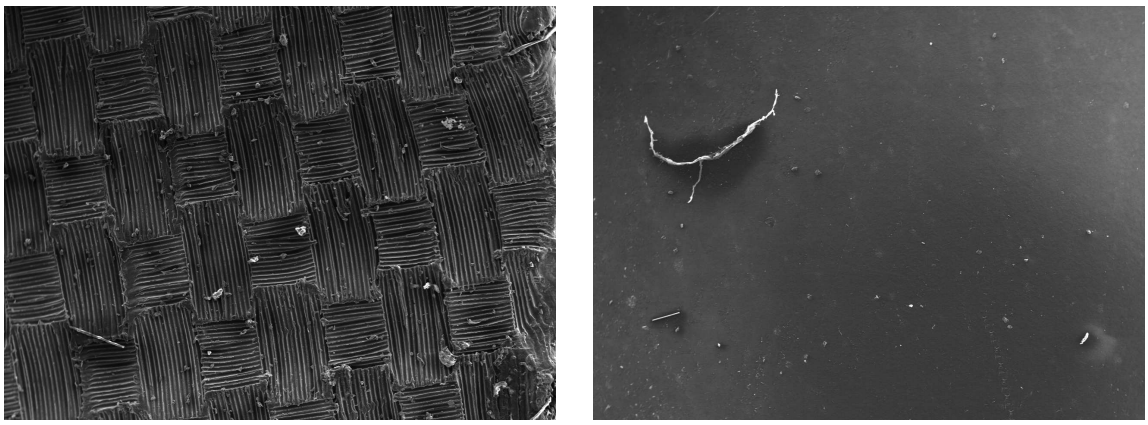

(a) **(b)**

Figure 5.17: SEM images of the surfaces of the ISL (a) and OSL (b). Differences in surface structure can be see, one example being the OSL showing a much smoother surface compared to the ISL where a repeating pattern can be seen. Differences in quantity of contaminants can also be seen where the ISL has a higher concentration of large contaminants. Both images were taken at 40x magnification with the width of the image corresponding to 3.2 mm.

5.9.1 Contaminants and Chemical Characterization

In Figure 5.17 a couple of different types of contaminants could be seen. Some of these are marked in different colors in Figure 5.18, and shown in more detail in the following section together with their EDS spectra. The EDS spectra were created by point measurements in the middle of the contaminants.

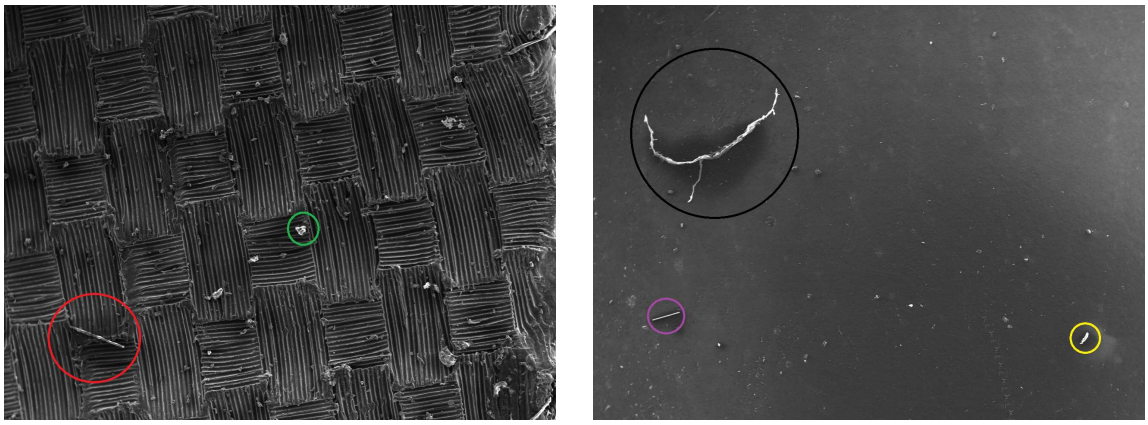

(a) **(b)**

Figure 5.18: Figure 5.17 but with some contaminants marked with different colors.

The contaminants looked at are divided into three different categories: contaminants from

the conductor band, threads and superabsorbent polymer powder from the swelling bands, and artifacts from the preparation or imaging process. Figures 5.19, and 5.20 show contaminants that fit into the conductor band category, Figures 5.21, 5.22 into the swelling bands category and Figure 5.23 into the artifacts from preparation and imaging.

The SEM images and the corresponding spectra for the conductor band contaminants can be seen below.

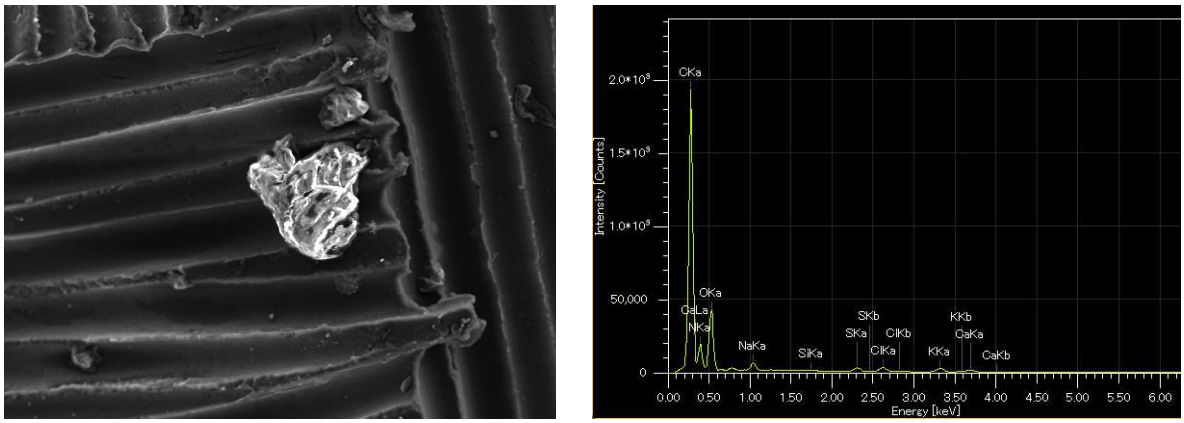

(a) **(b)**

Figure 5.19: The contaminant from Figure 5.18 marked with a green circle. a) shows an SEM image while b) shows its corresponding EDS spectrum that was taken from a point in the middle of the contaminant. The width of the image corresponds to 284 μm.

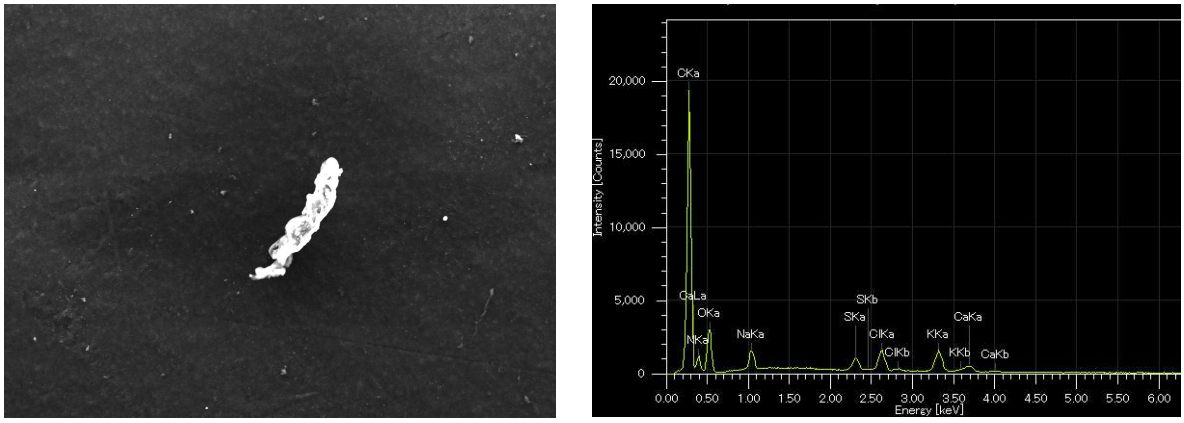

(a) **(b)**

Figure 5.20: The contaminant from Figure 5.18 marked with a yellow circle. a) shows an SEM image while b) shows its corresponding EDS spectrum that was taken from a point in the middle of the contaminant. The width of the image corresponds to 298 μm.

The percentages of the different elements present for conductor band contaminants are

detailed below in Table 5.3.

Table 5.3: Elemental composition of the conductor band contaminants.

Figure #	C	N	O	Na	Mg	Al	Si	P	S	Cl	K	Ca	Ti	Sum
5.19	49.52	20.91	26.03	0.88			0.05		0.51	0.71	0.84	0.54		100.00
5.20	55.27	15.45	17.83	1.91					1.44	2.82	3.91	1.37		100.00

The defining characteristic for this type of contaminant is the large percentage of nitrogen. The conductor bands are the only part of the cable that have nitrogen, making it easy to classify these contaminants. Something initially unexpected is that Figure 5.20 shows a conductor band contaminant on an OSL sample. This is weird as the conductor bands are only found next to the ISL but can simply be explained by cross-contamination.

The SEM images and the corresponding spectra for the swelling band contaminants can be seen below.

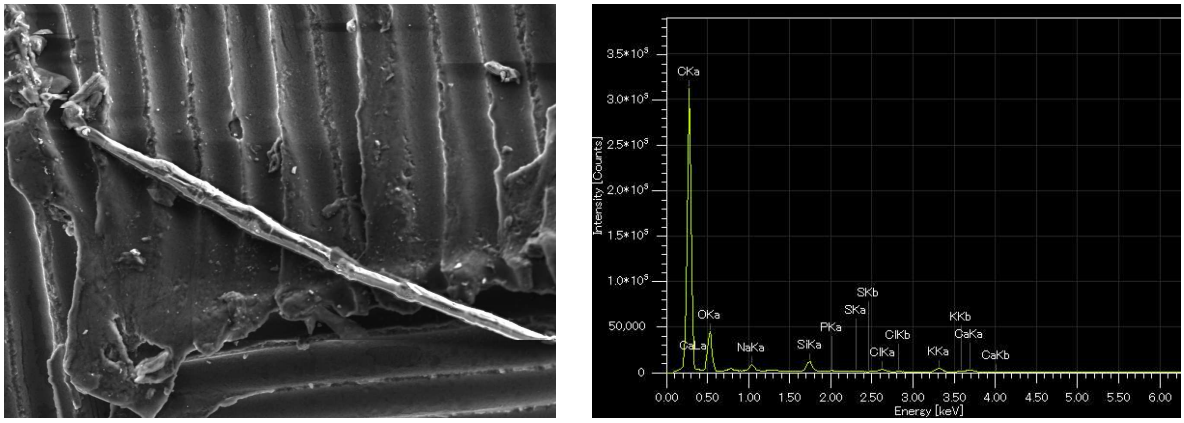

(a) **(b)**

Figure 5.21: The contaminant from Figure 5.18 marked with a red circle. a) shows an SEM image while b) shows its corresponding EDS spectrum that was taken from a point in the middle of the contaminant. The width of the image corresponds to 346 μm.

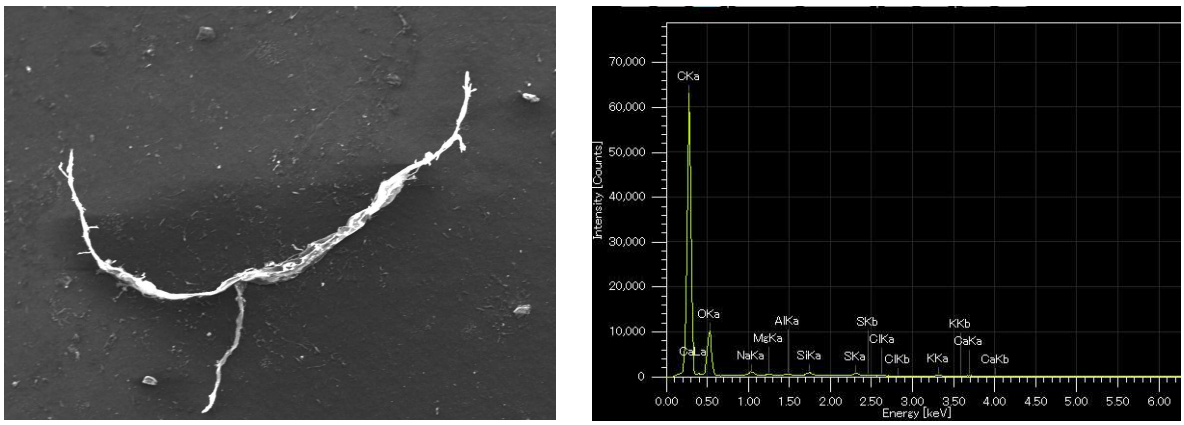

(a) **(b)**

Figure 5.22: The contaminant from Figure 5.18 marked with a black circle. a) shows an SEM image while b) shows its corresponding EDS spectrum that was taken from a point in the middle of the contaminant. The width of the image corresponds to 1 mm.

The percentages of the different elements present for swelling band contaminants are detailed below in Table 5.4.

Table 5.4: Elemental composition of the swelling band contaminants.

Figure #	C	N	O	Na	Mg	Al	Si	P	S	Cl	K	Ca	Ti	Sum
5.21	72.05		22.74	0.99			1.35	0.16	0.16	0.55	1.24	0.77		100.00
5.22	71.14		26.71	0.57	0.12	0.11	0.36		0.47	0.14	0.18	0.18		100.00

These contaminants are not as easily identified. The swelling bands themselves primarily contain C and O, the same as the semi-conducting layer itself. The main identifiers are the general appearance of the contaminants and all of the small amounts of other elements. Elements such as Na, K, and Ca are all commonplace in the superabsorbent polymer powder. Table 5.4 also shows signs of Mg and Al. Both aluminum and magnesium are common elements when constructing SEMs and their holders and are therefore likely an artifact from the tool itself.

The SEM image and its corresponding spectrum for artifacts from preparation and imaging can be seen below.

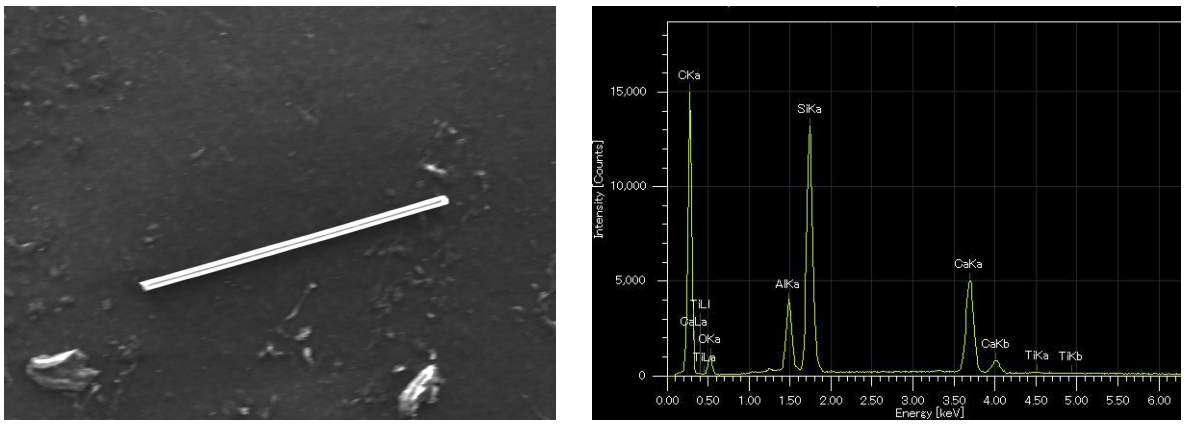

(a) **(b)**

Figure 5.23: The contaminant from Figure 5.18 marked with a purple circle. a) shows an SEM image while b) shows its corresponding EDS spectrum that was taken from a point in the middle of the contaminant. The width of the image corresponds to 284 μm.

The data from the final category of artifacts from preparation and imaging can be seen below in Table 5.5.

Table 5.5: Elemental composition of the artifacts from preparation and imaging contaminant.

Figure #	C	N	O	Na	Mg	Al	Si	P	S	Cl	K	Ca	Ti	Sum
5.23	60.55		5.74			3.89	14.17					15.42	0.22	100.00

This contaminant shows significant amounts of Al, Si, and Ti, all of which are common elements in tools like SEMs. They could also come from the sample holder or other tools used when preparing the samples themselves. The high amount of calcium could indicate that this is another element that is an artifact from the preparation and measuring and that the calcium in the other contaminants could also come from this.

In general both the amount and severity of contaminants are quite low. One aspect to them that could potentially be a cause of worry is the presence of S in both the conductor and swelling band contaminants. As discussed in section 3.4.1 silver-sulfur reactions could degrade the quality of contacts but the concentrations are so low that this does not seem like a problem.

Performing EDS analysis on the entire regions seen in Figures 5.18a and 5.18b gives an idea of how prevalent contaminants are. Spectra for these scans are seen below in Figure 5.24.

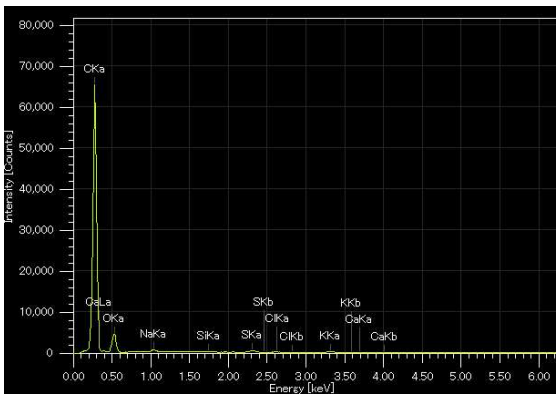

(a) EDS spectrum for the entire region in Figure 5.18a.

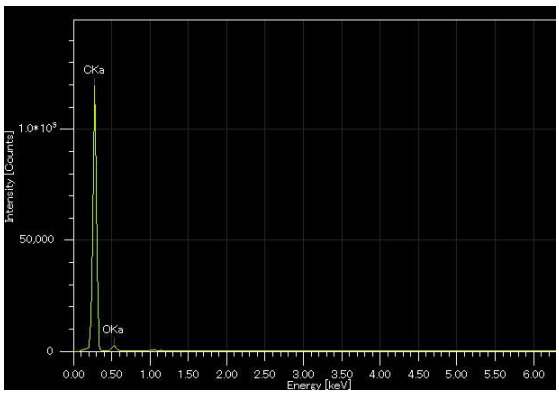

(b) EDS spectrum for the entire region in Figure 5.18b

Figure 5.24

From these spectra contaminants seem more common on the ISL than the OSL. This seems reasonable as not only is the OSL more thoroughly cleaned but the ISLs proximity to both the conductor and swelling bands means there are simply more sources of contaminants. In general, however, the concentration of the contaminants is quite low with only trace amounts being found.

5.9.2 Imaging of Contacts

The contact resistance partially depends on the topology and morphology of the contacts, using SEM one can study these aspects of both ISL and OSL samples. It can also give an idea of the coverage of the SCP. Below, in Figure 5.25 four SEM images of the silver contacts, both using the secondary electron detector and the back-scatterered topology mode can be seen.

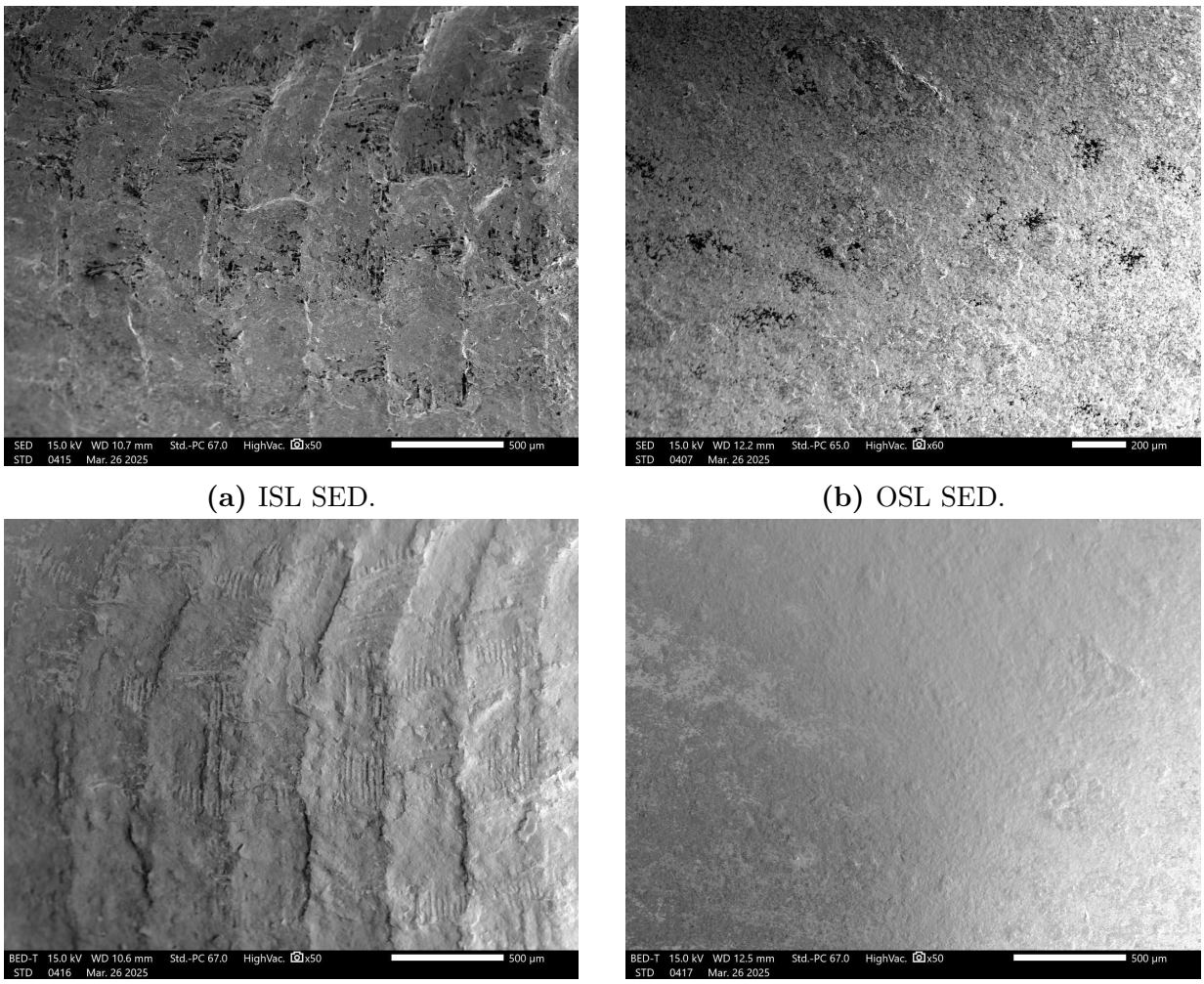

(a) ISL SED. **(b)** OSL SED.

(c) ISL BS-TOPO. **(d)** OSL BS-TOPO.

Figure 5.25: Four figures showing SEM imaging of the silver contacts. The upper row shows secondary electron imaging of the ISL and OSL respectively. The lower row shows the back-scattered topographical signal, once again of ISL and OSL respectively.

These images are quite promising. Most of the advanced weave-like structure seen for ISL samples, along with contaminants for both ISL and OSL, are not present in these SEM image. For the OSL, the surface is flat and completely covered in the silver. The ISL surface, on the other hand still shows remnants of the underlying structure, although the differences in height are not as significant as before the SCP was applied.

The SCP covers most of the sample with only some minor spots not being covered. A conclusion that can be drawn from this is that method for applying the SCP is quite satisfactory.

5.10 General Discussion of Results and Error Analysis

There is a clear difference between ISL and OSL samples, regardless of which parameter was being studied. This might seem odd as the same material is used for both layers, but there are some clear differences in fabrication between the two.

The biggest difference between ISL and OSL samples is naturally the shape and mass difference of the samples. ISL samples consist of half a cylinder with no conducting core, while OSL samples are whole cylinders with a conducting core. This leads to an enormous mass difference of almost a factor 10 ($\approx 0.85kg$ for ISL samples and $\approx 7kg$ for OSL samples). As seen in the SEM analysis of the samples, such as Figure 5.17, there are also differences in the topology of the ISL and OSL. The ISL, being closely packed to the conductor bands, get imprinted by their pattern. The same is not the case for the outer semi-conducting layer. A final difference between them is that OSL samples are thoroughly cleaned using conventional methods, such as scrubbing with dish soap, resulting in lower concentrations of contaminants while ISL samples are not.

There are a couple of things to consider that could have contributed to errors both small, changing the results by a some factor, or large, introducing uncertainties that question the accuracy of a measurement.

One inaccuracy that permeates the entire thesis is describing everything in terms of resistivity when resistance would probably be more accurate. The difference between resistance and resistivity is, as seen in Equation 3.3, just a factor of some geometric properties. Everything that has been referred to as resistivity throughout this thesis has been the resistance multiplied by the initial geometric factor at room temperature. This means that for every measurement there is a small error, that increases with temperature, due to the discrepancy between the initial and current geometric properties. If the dimensions of the sample could be continually updated throughout the measurement more accurate results could be obtained. This would, however, be an herculean task as not only would the temperature of the semi-conducting layers have to accurately kept up to date, from which the thermal expansion calculated and geometric properties updated, but the same would go for the insulation as its expansion also affects the dimensions of the semi-conducting layer.

As a consequence of the discrepancy between the "real" resistivity and the measured resistivity, the dimensions of the sample start mattering. Normally, resistivity is an intensive quality, meaning that it does not depend on the volume of the sample while resistance is an extensive quality, depending on the volume. This does not hold when the resistivity is calculated from the resistance as the resistivity now depends on an extensive quality.

Something that has been continuously seen in many measurements is how the resistivity has kept on either increasing or decreasing for a long time, even after the semi-conducting layer has reached thermal equilibrium. As previously discussed, one explanation for this is

the thermal expansion of the rest of the cable. This thermal expansion in turn pushes on the semi-conducting layer either increasing the thickness of it for ISL samples, or decreasing it for OSL samples. This change of thickness does not affect resistivity but does affect the resistance. As the measured resistivity depends on resistance it would, as opposed to the actual resistivity, also be affected by this. Therefore it is possible that the changes in resistivity seen after a couple of hours could just be changes in resistance but not actual resistivity.

Even though the measured and calculated resistivity has its issues, and would probably be more accurately described by using resistance, it still gives reasonable values of the actual resistivity as in most cases the changes in diameter and thickness are still relatively minor. It is simply something that should be kept in mind when discussing results.

One of the smaller potential errors comes from difficulties in measuring the thickness of the semi-conducting layers. When looking at Equation 3.3 we can see that the resistivity is proportional to a geometrical factor of $(d - t) \cdot t$. The thickness of the semi-conducting layers can vary quite a bit around the circumference making it difficult to have a realistic value of t. The variation in thickness can, for example, be about 30 % larger at the thickest sections compared to the thinnest. This can make it a bit difficult to precisely determine a t that would give perfect results.

Another difficulty comes from difficulties in measuring the temperature of the semi-conducting material. The method used provides results that seem reasonable, but since only one point was measured it is difficult to say how well the measured temperature represents the material at large. As discussed, the temperature plays a considerable role in the conductive abilities of the semi-conducting material and if a large temperature gradient was present throughout the material it could affect the results.

Inaccuracies could also occur from contact resistance or other difficulties with the contacts. Thankfully, due to using a four-point probe method with measurements performed at a set current, contact resistance is theoretically not something that will have had a large, if any, effect on results.

Something that was noticed for a large fraction of the measurements was that the samples had moved by upwards of 5 mm during the measurement. This movement was more clearly pronounced for OSL samples. This movement could come as a result of the thermal expansion or a slight melting of the sample or the careless handling of the measurement rigs as they were inserted into the measuring areas. The temperature effect explanation seems more significant as, in general, the motion away from the probes was clearer for measurements performed at higher temperatures.

Whatever the reason, this lead to the contacts getting shifted away from the probes. The consequences of this do not seem to be too severe. Although it is not known exactly when this movement away from the probe happened, making it more difficult to connect it to some behavior seen in the results, it seems likely that it can be connected to the unstable, fluctuating, behavior seen in some graphs. One clear example of this would be in Figure

5.5 which is shown below for the convenience of the reader.

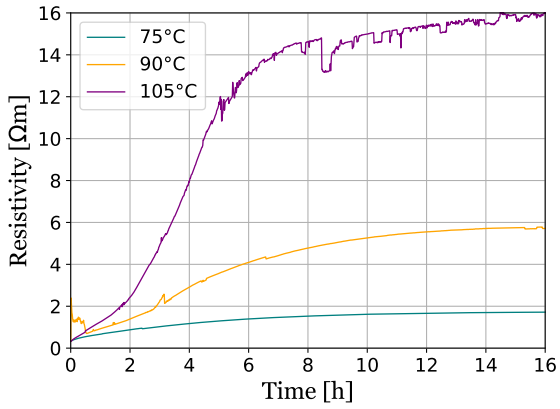

Figure 5.26: "The resistivity of OSL samples as a function of time for three different temperatures, 75, 90, and 105 $°C$." This figure and caption was previously seen in Figure 5.5 and is reprinted here for the convenience of the reader.

In the 105 $°C$ plot an erratic behavior starts being seen after $\approx$ 5 hours. Before this, the plot was quite smooth, making the contrast even clearer. The 90 $°C$ plot also shows some unstableness throughout the entire measurement but to a much smaller degree while the 75 $°C$ plot is very smooth. The magnitude of this noise is relatively small in effect, about 10 % of the total magnitude.

A simple experiment was conducted to get a better understanding of the effect that disconnects between probes and contacts had on the resistivity. ISL and OSL samples were placed on the rig as during a normal measurement and the resistivity was measured every 10 seconds for a period of 15 minutes at room temperature. The samples were then shifted $\approx$ 1 cm such that none of the probes touched contacts and the resistivity measurement was performed again. Each of these measurements were performed twice. The results from these measurements can be seen below in Figure 5.27.

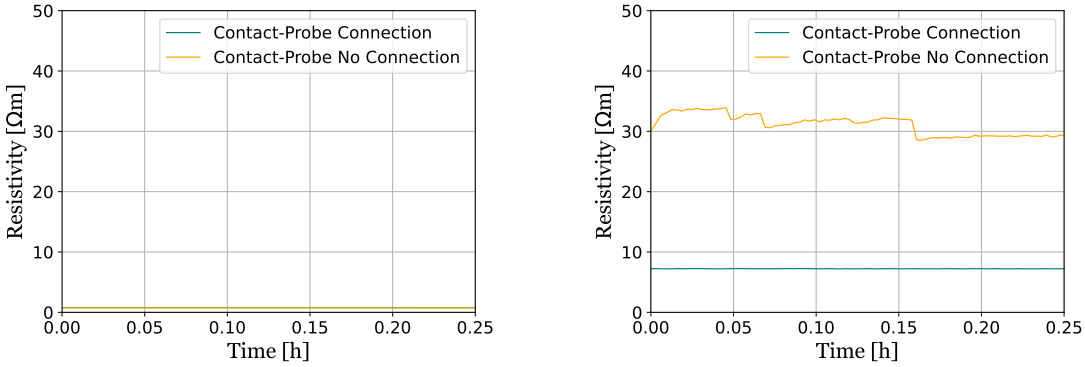

(a) Two short ISL measurements comparing the resistivity when the probes and contacts are connected and when they are not.

(b) Two short OSL measurements comparing the resistivity when the probes and contacts are connected and when they are not.

Figure 5.27

For the ISL results there was seemingly no difference between the results when the probes and contacts were in contact, and when they were not. This is the desired result when using a four-point probe method as it should bypass contact resistance.

The OSL results, on the other hand, show significant differences. Not only is the resistivity larger when the probes and contacts are not touching, but it is also much more unstable, fluctuating during the entire measurement and never reaching an especially stable value. Something to note is that the "Contact-Probe connection" measurement has a very large resistivity compared to typical OSL results. This should, however, not affect the larger change in resistivity seen between the "Contact-Probe Connection" and "Contact-Probe No Connection" measurements.

This short experiment compared the scenarios when all probes and contacts being in contact to when none of them were connected. This differs from typical measurements where usually only one or two contacts become disconnected. Regardless of these differences from an actual measurement this still seems like a valid explanation to why some OSL results fluctuate and why large jumps in resistivity can occasionally be seen. It also shows the importance of having the good contacts and makes it clear that the OSL side of the rig leaves a lot to be desired.

The K-type thermocouple wire that was used for the measurements also had its issues as it was both difficult to use and had not been calibrated. For a thermocouple wire to accurately read temperature, the two wires of different metals within it have to touch each other at the point where the temperature is measured. It was relatively common that the contact between the wires would be broken when the wire was inserted into the measuring area, making the measurement useless. This could usually be noticed immediately when the measurement was initiated and easily fixed by simply redoing the measurement. The

lack of calibration seems like a relatively minor issue as both the starting and end values are mostly correct and the rest of the result seems reasonable.

Due to measurements being performed for long periods of time, 16 hours, there only being one measuring rig with SMU, and the large amount of different aspects that were studied, it was difficult to obtain the desired amount of measurements. Ideally, with more time and resources, at least three measurements per measuring point would have been done to increase the consistency of results. This was done to some degree, with almost every measurement being repeated at least once, and sometimes twice but once again, more repeated measurements would naturally be better. During the project there were longer periods of time where the measuring equipment was not available due to calibration and other such things that exacerbated the problem of not having enough time for all the measurements. In hindsight, it may have been smart to slightly decrease the scope of the thesis to make sure that all measurements would have more backup measurements to increase the accuracy of the results.

Unfortunately, the thermocouple wire used to conduct temperature measurements was not obtained until more than 2 months into the project. As a consequence the amount of temperature measurements was quite limited. Furthermore, the equipment was only available every other week which further decreased the amount of temperature measurements. On a more positive note, the variation in how different samples heated was significantly smaller than the variation observed for their resistivity. Nearly all ISL measurements exhibited the same thermal behavior, as did the OSL measurements. Ideally this would mean that any given 90 $^{\circ}C$ temperature measurement would be able to accurately describe all others performed at the same temperature, counteracting the inaccuracies from a lower amount of total measurements.

6 Conclusion

In this thesis the mechanics behind resistivity measurements for the semi-conducting layers in HVDC cables have been discussed in detail. 16 hour long measurements were performed and had their results discussed on different semi-conducting samples in varying conditions such as: different temperatures, using a constant measuring current contra a periodic measuring current, alternate methods of preparing samples, cross-linked samples and non cross-linked samples, different types of semi-conducting materials, and different values of relative humidity. The measurements that initiated the creation of this thesis were also successfully recreated. The incredibly high resistivity values that were obtained in the introductory measurements seem to be a consequence of that specific cable/semi-conductor material rather than something systematic with multi-hour measurements. SEM and EDS analysis was also performed on the samples to get a better understanding of the material, potential contaminants, its surface, and its composition. A detailed description of the physics of the semi-conducting material was also provided which was then used to explain results.

All pertinent measurements were successfully performed and for each of these the results were thoroughly discussed and explanations for the results were put forth. Both theoretical explanations, and more practical explanations connected to the methodology were detailed. All important parts of the results were discussed: the transitionary region at the start, the stabilization and steady state, and the long term effects seen after many hours. Some difficulties with the methodology were also discussed.

These results can help further develop the testing methodology, improving results, and deepening the understanding of semi-conducting measurements. Improving the efficiency and understanding of testing methodology can hopefully, in turn, further the development of cheaper, and more efficient semi-conductor materials for HVDC cables.

7 Outlook

Even though this thesis has examined semi-conducting materials in many different contexts, many remain unexamined, or not examined to their full extent.

In many of the ISL measurements there has been a clear trend where the resistivity continues decreasing by a small amount, even after 16 hours had elapsed. If this project were to be continued it would be interesting to examine for how long this decrease in resistivity continues. The same goes for OSL measurements where a clear, but small, increase of resistivity could be seen after the sample had supposedly reached thermal equilibrium.

For temperature measurements it would be interesting to expand the scope of measurements, including more extreme values. The temperatures used for the thesis were chosen to be either at, or close to the standard measuring temperature (90 $°C$). Choosing temperatures further away from this temperature would not be as relevant for the purpose of understanding HVDC cables but could, nevertheless, be interesting. A single measurement of this character was performed at 120 $°C$ and can be seen below in Figure 7.1.

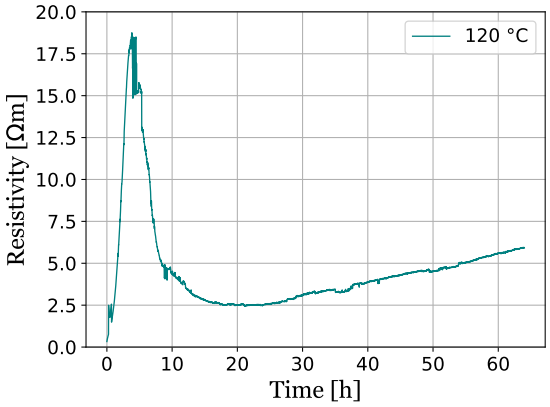

Figure 7.1: The resistivity of an OSL sample at 120 $°C$ over a duration of 64 hours.

This graph shows both the PTC and NTC as discussed in section 3.3.2 and would be very interesting to study further.

Also related to temperature, it would be interesting to get a more detailed perspective on the temperature gradient throughout both the entire semi-conducting layer and the rest of the cable. During this project the temperature was measured at a single point towards the edge of the cable in the middle of semi-conducting layer. This does not give any information about neither the insulation layer nor the rest of the semi-conducting material. Differences in temperature throughout the semi-conducting layer could naturally affect results and

having a better grasp on the temperature of the insulation layer could give a better idea of the speed at which thermal expansion of this layer occurs. Performing a more extensive study of temperature throughout the cable could both improve the quality of the results and general understanding of the testing methodology and its details.

Another thing that could be expanded on in further studies is the effectiveness of the sample preparation and measuring methodology. Many of the graphs throughout the thesis have some sort of irregularities and in many cases it can be difficult to know whether the irregularity came from some material property or simply a measuring error.

One possible explanation that was put forth for these irregularities was contact resistance and errors arising from the contacts and probes getting separated. This was discussed to some degree in the paragraphs around Figure 5.27. This is another subject of interest for further study. It would be interesting to expand on this measurement and see how the results are affected by having, for example one or multiple probes separated from the contacts instead of just the simple measurement where all probes were separated. Furthermore, other aspects of the contacts could also be examined such as their thickness and the amount of layers of SCP.

In section 5.10 some differences between cables in actual use compared to the samples used for testing in this thesis were put forth. Out of these, it would perhaps be the most interesting to survey how the semi-conducting layers would react to a voltage being put over the conductive core. The electric field generated by this could potentially affect resistivity properties. This would of course be quite difficult to do and a different methodology, following different IEC standards would have to be used.

Finally, it could also be interesting to compare differences between measuring the semi-conducting material as a part of a processed cable or just by itself. As previously discussed, it seems very likely that at least some behaviors of the semi-conducting layer at elevated temperatures can be described by thermal expansion of the insulating layer. These effects would disappear if measurements were performed on an individual plate of the semi-conducting material. Some of the contaminants seen on the semi-conducting material also came from the adjacent conductor and swelling bands, these would not be seen when simply measuring a plate of the semi-conducting material. Some aspects that could be beneficial to study are:

- The resistivity of a plate of semi-conducting material with the same thickness and surface area as a normal sample.
- The heating of a plate of semi-conducting material and the heat-resistivity coefficient.
- The resistivity of a plate with some applied external electrical field.

8 Confidentiality, Conflicts of Interest, and Ethical Disclosure

This work was performed as a part of a temporary employment at NKT HV Cables AB (559079-0290), as a result some material and process specific details are omitted. Payment was also received for the finished work and living arrangements were also provided by NKT.

Minor parts of the project have been omitted due to confidentiality reasons, almost exclusively from section 5.5.

AI LLM tools were used for minor re-phrasings and grammar corrections along with generating BibTeX citations from some sources. The AI tools' role in this second part was limited to just creating the citations and it was not involved with finding, interpreting, or analyzing any of the sources. Everything that the AI tools created was also manually double checked.

Bibliography

[1] E. Law. *Can We Eliminate These 3 Types of Line Losses in Transmission Systems?* Accessed: 2025-02-27. 2022. URL: https://www.cencepower.com/blog-posts/line-losses-power-transmission-3-types.

[2] ZMS Cable. *What are the applications of high voltage cables?* Accessed: 2025-02-26. 2022. URL: https://www.zmscable.com/news/what-are-the-applications-of-high-voltage-cables.

[3] Michael. *High Voltage Power Cables: An In-Depth Introduction.* Accessed: 2025-02-26. 2025. URL: https://www.eescable.com/news/high-voltage-power-cables-an-in-depth-introduction.

[4] R. Zi. *High Voltage Cable: Everything You Need to Know.* Accessed: 2025-02-26. 2023. URL: https://www.centralwires.com/high-voltage-cable-everything-you-need-to-know/.

[5] ZMS Cable. *Why High Voltage Cables Don't Have an Insulation Layer?* Accessed: 2025-02-26. 2023. URL: https://zmscable.es/en/cables-alta-tension-no-aislamiento/.

[6] EES Cable. *Different between Low and High voltage cables?* Accessed: 2025-02-27. 2025. URL: https://www.eescable.com/different-between-low-and-high-voltage-cables/.

[7] National Grid. *Undergrounding High Voltage Electricity Transmission Lines: The Technical Issues.* Accessed: 2025-02-27. 2015. URL: https://www.nationalgrid.com/sites/default/files/documents/39111-Undergrounding_high_voltage_electricity_transmission_lines_The_technical_issues_INT.pdf.

[8] ZMS Cable. *Development history of power cables.* Accessed: 2025-05-06. 2023. URL: https://m.zmscable.com/new/Development-history-of-power-cables.

[9] ELEK. *Summary of Electric Power Cable History.* Accessed: 2025-05-06. 2025. URL: https://elek.com/articles/summary-of-electric-power-cable-history/#elementor-toc__heading-anchor-3.

[10] SPARK: Museum of Electrical Invention. *"Edison Tube" Electrical Distribution Cable.* Accessed: 2025-05-06. 2023. URL: https://www.sparkmuseum.org/portfolio-item/edison-tube-electrical-cable/.

[11] F. Pirelli. *Pirelli: Stories of People and Inventions: Luigi Emanueli.* Accessed: 2025-05-06. 2020. URL: https://www.fondazionepirelli.org/en/historical-archive/pirelli-storie-di-uomini-e-di-invenzioni-luigi-emanueli/.

[12] NKT. *Doubling power transmission over longer distances.* Accessed: 2025-05-06. 2023. URL: https://www.nkt.com/products-solutions/high-voltage-cable-solutions/innovation/525-kv-extruded-hvdc-cable-systems.

[13] U.S. Department of Energy. *The War of the Currents: AC vs. DC Power.* Accessed: 2025-05-06. 2014. URL: https://www.energy.gov/articles/war-currents-ac-vs-dc-power.

[14] National Grid. *High Voltage Direct Current Electricity – Technical Information*. Accessed: 2025-02-27. 2025. URL: https://www.nationalgrid.com/sites/default/files/documents/13784-High%20Voltage%20Direct%20Current%20Electricity%20%E2%80%93%20technical%20information.pdf.

[15] Polycab India Limited. *Energy and Power Grid - Renewable Energy*. Accessed: 2025-02-27. 2025. URL: https://polycab.com/cables/applications/energy-and-power-grid/renewable-energy.

[16] Cableworld Ltd. *AC vs DC Cables: Understanding the Difference*. Accessed: 2025-04-08. 2024. URL: https://www.cable-world.co.uk/ac-vs-dc-cables-understanding-the-difference/.

[17] R. Günther. *AC vs DC: Which System is Better Suited for Modern Energy Needs?* Accessed: 2025-05. 2024. URL: https://clouglobal.com/ac-vs-dc-which-system-is-better-suited-for-modern-energy-needs/.

[18] E. Law. *4 Reasons Power Grids Still Distribute AC Electricity*. Accessed: 2025-05-06. 2022. URL: https://www.cencepower.com/blog-posts/4-reasons-power-grids-still-distribute-ac-electricity.

[19] M. Severengiz, T. Sprenger, and G. Seliger. "Challenges and Approaches for a Continuous Cable Production". In: *Procedia CIRP* 40 (Dec. 2016), pp. 18–23. DOI: 10.1016/j.procir.2016.01.040.

[20] A. Metwally. *HV High Voltage Cables: Standardization and Optimization of High Voltage Cables Design*. Accessed: 2025-02-26. 2019. URL: https://www.powerandcables.com/hv-high-voltage-cables/.

[21] NKT. *High Voltage Offshore DC Cables*. Accessed: 2025-02-26. 2025. URL: https://www.nkt.com/products-solutions/high-voltage-cable-solutions/high-voltage-offshore-solutions.

[22] Guanxi Zhongwei Cable. *Introduction to the Basic Knowledge of Conductor Shielding Layer and Metal Shielding Layer*. Accessed: 2025-04-09. 2024. URL: https://www.zhongweicables.com/news/introduction-to-the-basic-knowledge-of-conductor-shielding-layer-and-metal-shielding-layer/.

[23] Alphagary. *Why Semi-Conductive Layers Matter in Medium- and High-Voltage Power Cables*. Accessed: 2025-04-08. 2024. URL: https://www.alphagary.com/post/why-semi-conductive-layers-matter-in-medium-and-high-voltage-power-cables.

[24] C. Dodds. *What Is Electrical Stress?* https://www.powerandcables.com/what-is-electrical-stress/. 2020.

[25] S. Soady. *The Purpose Of The Screen & Semi-conductive Layer On MV Cables*. https://www.powerandcables.com/screen-semi-conductive-layer-on-mv-cables/. 2020.

[26] J. Sun. *Why High Voltage Cables Need Semiconductor Layers*. https://zoliov.com/why-high-voltage-cables-semiconductor-layer/. 2025.

[27] C.G. Richardson. "Compounding of Semiconductives for High Voltage Cables". In: *Jicable'07*. 2007.

[28] Y. Wei et al. "Effect of temperature on electric-thermal properties of semi-conductive shielding layer and insulation layer for high-voltage cable". In: *High Voltage* 6.5 (2021), pp. 805–812. DOI: https://doi.org/10.1049/hve2.12089. URL: https://ietresearch.onlinelibrary.wiley.com/doi/abs/10.1049/hve2.12089.

[29] Anixter Inc. *Cable Jacket Types 101*. Accessed: 2025-03-25. 2025. URL: https://www.anixter.com/en_us/resources/literature/wire-wisdom/cable-jackets-types-101.html.

[30] D. Fabiani et al. "Polymeric HVDC Cable Design and Space Charge Accumulation. Part 1: Insulation/Semicon Interface". In: *IEEE Electrical Insulation Magazine* 23.6 (2007), pp. 11–19. DOI: 10.1109/MEI.2007.4389975.

[31] J. Parmar. *Cable Construction & Cable Selection - Part:1*. Accessed: 2025-04-08. 2016. URL: https://electricalnotes.wordpress.com/2016/04/07/cable-construction-cable-selection-part1/.

[32] S. Delpino et al. "Feature article - Polymeric HVDC cable design and space charge accumulation. Part 2: insulation interfaces". In: *IEEE Electrical Insulation Magazine* 24.1 (2008), pp. 14–24. DOI: 10.1109/MEI.2008.4455499.

[33] Y. Özüpak. "Analysis of the Effect of Air Gaps on the Electric Field in the Insulation Material of High Voltage Transmission Cables". In: *Erzincan University Journal of Science and Technology* 15 (2022), pp. 69–79. DOI: https://doi.org/10.18185/erzifbed.952750. URL: https://dergipark.org.tr/en/pub/erzifbed/issue/69107/952750.

[34] Orbia. *ESCONTEK: Semi-conductive compounds for MV and HV power cables*. https://www.alphagary.com/semi-conductive-compounds. 2025.

[35] J. Su et al. "Effects of Mechanical Stress on Insulation Structure and Performance of HV Cable". In: *Polymers* 14.14 (2022). ISSN: 2073-4360. DOI: 10.3390/polym14142927. URL: https://www.mdpi.com/2073-4360/14/14/2927.

[36] BUSS. *Semi Conductive Cable Compounding*. https://busscorp.com/industries/semiconductive-cable-compounds/. 2025.

[37] ENTEC. *Ethylene Butyl Acrylate Copolymer (EBA)*. https://www.entecpolymers.com/products/resin-types/ethylene-butyl-acrylate-copolymer-eba. 2025.

[38] HANWHA. *The ABCs of EBA: The Role of Ethylene Butyl Acrylate in the Energy Transition*. https://www.hanwha.com/newsroom/news/feature-stories/the-abcs-of-eba-the-role-of-ethylene-butyl-acrylate-in-the-energy-transition.do. 2023.

[39] DOW. *ELVALOY™ AC 3717 Acrylate Copolymer*. https://www.dow.com/en-us/pdp.elvaloy-ac-3717-acrylate-copolymer.1891598z. 2025.

[40] S. Fromentin. *Resistivity of Carbon, Diamond*. https://hypertextbook.com/facts/2004/KerryRemulla.shtml. 2004.

[41] A. Belgrave. *Resistivity of Carbon, Graphite*. https://hypertextbook.com/facts/2004/AfricaBelgrave.shtml. 2004.

[42] S. Banerjee and A.K. Tyagi. *Functional Materials: Preparation, Processing and Applications*. Elsevier, 2011.

[43] K. Hardyal. *What Is graphitization? A Carbon/Graphite Engineer Explains*. https://blog.metcar.com/what-is-graphitization. 2020.

[44] DENKA. *DENKA BLACK*. https://www.denka.co.jp/eng/product/detail_00025/. Carbon Black Product. 2025.

[45] S. Perkins. *Explainer: What are polymers?* https://www.snexplores.org/article/explainer-what-are-polymers. 2017.

[46] D. C. Giancoli. *Physics*. 4th. Englewood Cliffs, N.J.: Prentice Hall, 1995. ISBN: 0131021532.

[47] I. Glowacki et al. "2.33 - Conductivity Measurements". In: *Polymer Science: A Comprehensive Reference*. Ed. by K. Matyjaszewski and M Möller. Amsterdam: Elsevier, 2012, pp. 847–877. ISBN: 978-0-08-087862-1. DOI: https://doi.org/10.1016/B978-0-444-53349-4.00058-3. URL: https://www.sciencedirect.com/science/article/pii/B9780444533494000583.

[48] Entec. *Repsol PRIMEVA EVA and EBANTIX EBA Copolymers*. https://www.entecpolymers.com/resources/product-guides/repsol-primeva-eva-and-ebantix-eba-copolymers. 2025.

[49] De Monchy. *EBA (Ethylene Butyl Acrylate)*. https://monchy.com/products/eba/. 2025.

[50] J. Maitra and V. Shukla. "Cross-linking in hydrogels - a review". In: *Am J Polym Sci* 4 (Jan. 2014), pp. 25–31.

[51] N. Li, L. Wang, and M. Hickner. "Cross-linked comb-shaped anion exchange membranes with high base stability". In: *Chemical Communications* 50.31 (2014), pp. 10141–10144. DOI: https://doi.org/10.1039/C3CC49027K.

[52] G. Nie et al. "Alkali resistant cross-linked poly(arylene ether sulfone)s membranes containing aromatic side-chain quaternary ammonium groups". In: *Journal of Membrane Science* 474 (2015), pp. 187–195. ISSN: 0376-7388. DOI: https://doi.org/10.1016/j.memsci.2014.09.053. URL: https://www.sciencedirect.com/science/article/pii/S0376738814007558.

[53] L. Wu et al. "Thermal crosslinking of an alkaline anion exchange membrane bearing unsaturated side chains". In: *Journal of Membrane Science* 490 (2015), pp. 1–8. ISSN: 0376-7388. DOI: https://doi.org/10.1016/j.memsci.2015.04.046. URL: https://www.sciencedirect.com/science/article/pii/S0376738815003774.

[54] S. Mashhadikhan et al. "Breaking temperature barrier: Highly thermally heat resistant polymeric membranes for sustainable water and wastewater treatment". In: *Renewable and Sustainable Energy Reviews* 189 (2024), p. 113902. ISSN: 1364-0321. DOI: https://doi.org/10.1016/j.rser.2023.113902. URL: https://www.sciencedirect.com/science/article/pii/S1364032123007608.

[55] A. Chapiro. "Radiation Effects in Polymers". In: *Encyclopedia of Materials: Science and Technology*. Ed. by K. H. J. Buschow et al. Oxford: Elsevier, 2004, pp. 1–8. ISBN: 978-0-08-043152-9. DOI: https://doi.org/10.1016/B0-08-043152-6/01918-5. URL: https://www.sciencedirect.com/science/article/pii/B0080431526019185.

[56] M.E. Spahr, R. Gilardi, and D. Bonacchi. "Carbon Black for Electrically Conductive Polymer Applications". In: *Fillers for Polymer Applications*. Ed. by R. Rothon. Cham: Springer International Publishing, 2017, pp. 375–400. ISBN: 978-3-319-28117-9. DOI: 10.1007/978-3-319-28117-9_32. URL: https://doi.org/10.1007/978-3-319-28117-9_32.

[57] S. Shenogin, Ferguson. L., and A.K. Roy. "The effect of contact resistance on electrical conductivity in filled elastomer materials". In: *Polymer* 198 (2020), p. 122502. ISSN: 0032-3861. DOI: https://doi.org/10.1016/j.polymer.2020.122502. URL: https://www.sciencedirect.com/science/article/pii/S0032386120303347.

[58] Y. Wei et al. "Research progress of semiconductive shielding layer of HVDC cable". In: *High Voltage* 5.1 (2020), pp. 1–6. DOI: https://doi.org/10.1049/hve.2019.0069. URL: https://ietresearch.onlinelibrary.wiley.com/doi/abs/10.1049/hve.2019.0069.

[59] C.G. Richardson. "COMPOUNDING OF SEMICONDUCTIVES FOR HIGH VOLTAGE CABLES". In: *JiCable* C5-1-2 (2007). URL: www.jicable.org/TOUT_JICABLE_FIRST_PAGE/2007/2007-C5-1-2_page1.pdf.

[60] J. Kim, N. Harris, and J. Tian. *The Roles of Carbon Black in Wire & Cable Conductor, Insulation and Jacketing Applications*. https://www.birlacarbon.com/the-roles-of-carbon-black-in-wire-cable-conductor-insulation-and-jacketing-applications/. 2021.

[61] J. Tian and R. Kamat. *Ensure Your Compound Comes Out Right: Seven Common Mistakes to Avoid*. https://www.birlacarbon.com/ensure-your-compound-comes-out-right-seven-common-mistakes-to-avoid/. 2018.

[62] I. Balberg. "Tunneling and nonuniversal conductivity in composite materials". In: *Phys. Rev. Lett.* 59 (12 Sept. 1987), pp. 1305–1308. DOI: 10.1103/PhysRevLett.59.1305. URL: https://link.aps.org/doi/10.1103/PhysRevLett.59.1305.

[63] S. Miyauchi and E. Togashi. "The conduction mechanism of polymer–filler particles". In: *Journal of Applied Polymer Science* 30.7 (1985), pp. 2743–2751. DOI: 10.1002/app.1985.070300703. URL: https://www.scopus.com/inward/record.uri?eid=2-s2.0-0022093352&doi=10.1002%2fapp.1985.070300703&partnerID=40&md5=043071272c74ebf6d208f84d1c1f24aa.

[64] K. Ohe and Y. Naito. "Anew resistor having an anomalously large positive temperature coefficient". In: *Japanese Journal of Applied Physics* 10.1 (1971). Cited by: 243, pp. 99–108. DOI: 10.1143/JJAP.10.99. URL: https://www.scopus.com/inward/record.uri?eid=2-s2.0-1542470130&doi=10.1143%2fJJAP.10.99&partnerID=40&md5=4e93690c92b62bb3b2fd2b4ae8050003.

[65] Matan. *How do conductors work?* Accessed: 2025-06-18. 2023. URL: https://www.electricity-magnetism.org/how-do-conductors-work/.

[66] Matan. *How does temperature affect electrical conductivity?* Accessed: 2025-06-18. 2023. URL: https://www.electricity-magnetism.org/how-does-temperature-affect-electrical-conductivity/.

[67] E. K. Sichel, J. I. Gittleman, and Ping Sheng. "ELECTRICAL PROPERTIES OF CARBON - POLYMER COMPOSITES". In: *J. Electron. Mater* 11 (July 1982),

pp. 699–747. DOI: https://doi.org/10.1007/BF02672392. URL: https://link.springer.com/article/10.1007/BF02672392.

[68] C. A. Nieves et al. "Electron transport mechanisms in polymer-carbon sphere composites". In: *Journal of Applied Physics* 120.1 (July 2016), p. 014302. ISSN: 0021-8979. DOI: 10.1063/1.4955166. URL: https://doi.org/10.1063/1.4955166.

[69] M. W. Ferralli and A. F. Lewis. "ELECTRICAL CHARGE TRANSPORT MECHANISMS IN CARBON BLACK FILLED GLASSY POLYMERS". In: *Phase Transitions–1973*. Ed. by H.K. HENISCH, R. ROY, and L.E. CROSS. Pergamon, 1973, pp. 409–422. ISBN: 978-0-08-017955-1. DOI: https://doi.org/10.1016/B978-0-08-017955-1.50042-7. URL: https://www.sciencedirect.com/science/article/pii/B9780080179551500427.

[70] M. B. Heaney. "Electrical transport measurements of a carbon-black—polymer composite". In: *Physica A: Statistical Mechanics and its Applications* 241.1 (1997). Proceedings of the Fourth International Conference on Electrical Transport and Optical Properties of Inhomogeneoous Media, pp. 296–300. ISSN: 0378-4371. DOI: https://doi.org/10.1016/S0378-4371(97)00098-8. URL: https://www.sciencedirect.com/science/article/pii/S0378437197000988.

[71] H Hexmoor. "Chapter 6 - Diffusion and Contagion". In: *Computational Network Science*. Ed. by H Hexmoor. Emerging Trends in Computer Science and Applied Computing. Boston: Morgan Kaufmann, 2015, pp. 45–64. ISBN: 978-0-12-800891-1. DOI: https://doi.org/10.1016/B978-0-12-800891-1.00006-8. URL: https://www.sciencedirect.com/science/article/pii/B9780128008911000068.

[72] V. Beffara and V. Sidoravicius. "Percolation Theory". In: *Encyclopedia of Mathematical Physics*. Ed. by J-P. Françoise, G.L. Naber, and T.S. Tsun. Oxford: Academic Press, 2006, pp. 21–28. ISBN: 978-0-12-512666-3. DOI: https://doi.org/10.1016/B0-12-512666-2/00202-9. URL: https://www.sciencedirect.com/science/article/pii/B0125126662002029.

[73] D. Ai et al. "Computer vision framework for crack detection of civil infrastructure—A review". In: *Engineering Applications of Artificial Intelligence* 117 (2023), p. 105478. ISSN: 0952-1976. DOI: https://doi.org/10.1016/j.engappai.2022.105478. URL: https://www.sciencedirect.com/science/article/pii/S0952197622004687.

[74] V. Duran et al. "Chapter 5 - Modeling epidemics based on quantum decision-making model by the qutrit states and employing neutrosophic form of percolation analysis". In: *Cognitive Intelligence with Neutrosophic Statistics in Bioinformatics*. Ed. by F. Smarandache and M. Aslam. Cognitive Data Science in Sustainable Computing. Academic Press, 2023, pp. 87–118. ISBN: 978-0-323-99456-9. DOI: https://doi.org/10.1016/B978-0-323-99456-9.00016-7. URL: https://www.sciencedirect.com/science/article/pii/B9780323994569000167.

[75] D. Zhukov et al. "Chapter 23 - Structural and Percolation Models of Intelligence: To the Question of the Reduction of the Neural Network". In: *Emerging Trends in Applications and Infrastructures for Computational Biology, Bioinformatics, and Systems Biology*. Ed. by Q.N. Tran and H.R. Arabnia. Emerging Trends in Com-

puter Science and Applied Computing. Boston: Morgan Kaufmann, 2016, pp. 333–340. ISBN: 978-0-12-804203-8. DOI: https://doi.org/10.1016/B978-0-12-804203-8.00023-7. URL: https://www.sciencedirect.com/science/article/pii/B9780128042038000237.

[76] M.J. Choi et al. "Electrical percolation threshold of carbon black in a polymer matrix and its application to antistatic fibre". In: *Scientific Reports* 9 (2019), p. 6338. DOI: 10.1038/s41598-019-42495-1.

[77] L.C. Costa and F. Henry. "DC electrical conductivity of carbon black polymer composites at low temperatures". In: *Journal of Non-Crystalline Solids* 357.7 (2011), pp. 1741–1744. ISSN: 0022-3093. DOI: https://doi.org/10.1016/j.jnoncrysol.2010.11.119. URL: https://www.sciencedirect.com/science/article/pii/S0022309311001165.

[78] J Sandler et al. "Development of a dispersion process for carbon nanotubes in an epoxy matrix and the resulting electrical properties". In: *Polymer* 40.21 (1999), pp. 5967–5971. ISSN: 0032-3861. DOI: https://doi.org/10.1016/S0032-3861(99)00166-4. URL: https://www.sciencedirect.com/science/article/pii/S0032386199001664.

[79] G. Grimmett. "What is Percolation?" In: *Percolation*. Berlin, Heidelberg: Springer Berlin Heidelberg, 1999, pp. 1–31. ISBN: 978-3-662-03981-6. DOI: 10.1007/978-3-662-03981-6_1. URL: https://doi.org/10.1007/978-3-662-03981-6_1.

[80] J.K.W. Sandler et al. "Ultra-low electrical percolation threshold in carbon-nanotube-epoxy composites". In: *Polymer* 44.19 (2003). In Honour of Ian Ward's 75th Birthday, pp. 5893–5899. ISSN: 0032-3861. DOI: https://doi.org/10.1016/S0032-3861(03)00539-1. URL: https://www.sciencedirect.com/science/article/pii/S0032386103005391.

[81] A. Celzard et al. "Critical concentration in percolating systems containing a high-aspect-ratio filler". In: *Physical Review B - Condensed Matter and Materials Physics* 53.10 (1996). Cited by: 500, pp. 6209–6214. DOI: 10.1103/PhysRevB.53.6209. URL: https://www.scopus.com/inward/record.uri?eid=2-s2.0-0001638405&doi=10.1103%2fPhysRevB.53.6209&partnerID=40&md5=d90c9a5bb2f2f8574a1e43af78d6641a.

[82] Stuart H. Munson-Mcgee. "Estimation of the critical concentration in an anisotropic percolation network". In: *Physical Review B* 43.4 (1991). Cited by: 205, pp. 3331–3336. DOI: 10.1103/PhysRevB.43.3331. URL: https://www.scopus.com/inward/record.uri?eid=2-s2.0-0001179888&doi=10.1103%2fPhysRevB.43.3331&partnerID=40&md5=bd90b6de921742e9c3ed75b038d7b3a0.

[83] M. Haghgoo, R. Ansari, and M.K. Hassanzadeh-Aghdam. "Predicting effective electrical resistivity and conductivity of carbon nanotube/carbon black-filled polymer matrix hybrid nanocomposites". In: *Journal of Physics and Chemistry of Solids* 161 (2022), p. 110444. ISSN: 0022-3697. DOI: https://doi.org/10.1016/j.jpcs.2021.110444. URL: https://www.sciencedirect.com/science/article/pii/S0022369721005102.

[84] Javad Payandehpeyman et al. "Physics-Based Modeling and Experimental Study of Conductivity and Percolation Threshold in Carbon Black Polymer Nanocom-

posites". In: *Applied Composite Materials* 31 (2024), pp. 127–147. DOI: https://doi.org/10.1007/s10443-023-10169-x. URL: %5Curl%7Bhttps://www.sciencedirect.com/science/article/pii/S002236972100510 2%7D.

[85] P Sheng, E. K. Sichel, and J. I. Gittleman. "Fluctuation-Induced Tunneling Conduction in Carbon-Polyvinylchloride Composites". In: *Phys. Rev. Lett.* 40 (18 May 1978), pp. 1197–1200. DOI: 10.1103/PhysRevLett.40.1197. URL: https://link.aps.org/doi/10.1103/PhysRevLett.40.1197.

[86] G.C. Psarras. "Hopping conductivity in polymer matrix–metal particles composites". In: *Composites Part A: Applied Science and Manufacturing* 37.10 (2006), pp. 1545–1553. ISSN: 1359-835X. DOI: https://doi.org/10.1016/j.compositesa.2005.11.004. URL: https://www.sciencedirect.com/science/article/pii/S1359835X05004057.

[87] T. Tamai. "Electric Contact Performances and Electrical Conduction Mechanisms of an Elastomeric Conductive Polymer". In: *Physicochemical Aspects of Polymer Surfaces: Volume 1*. Ed. by K. L. Mittal. Boston, MA: Springer US, 1983, pp. 507–520. ISBN: 978-1-4615-7584-9. DOI: 10.1007/978-1-4615-7584-9_29. URL: https://doi.org/10.1007/978-1-4615-7584-9_29.

[88] K-M. Jäger et al. "Electron transport and ac electrical properties of carbon black polymer composites". In: *Journal of Physics D: Applied Physics* 34.17 (Aug. 2001), p. 2699. DOI: 10.1088/0022-3727/34/17/319. URL: https://dx.doi.org/10.1088/0022-3727/34/17/319.

[89] G. C. Psarras. "Charge transport properties in carbon black/polymer composites". In: *Journal of Polymer Science Part B: Polymer Physics* 45.18 (2007), pp. 2535–2545. DOI: https://doi.org/10.1002/polb.21278. URL: https://onlinelibrary.wiley.com/doi/abs/10.1002/polb.21278.

[90] M. E. Spahr and R. Rothon. "Carbon Black as a Polymer Filler". In: *Polymers and Polymeric Composites: A Reference Series*. Ed. by Sanjay Palsule. Berlin, Heidelberg: Springer Berlin Heidelberg, 2016, pp. 1–31. ISBN: 978-3-642-37179-0. DOI: 10.1007/978-3-642-37179-0_36-2. URL: https://doi.org/10.1007/978-3-642-37179-0_36-2.

[91] C Zhang et al. "Temperature dependence of electrical resistivity for carbon black filled ultra-high molecular weight polyethylene composites prepared by hot compaction". In: *Carbon* 43.12 (2005), pp. 2544–2553. ISSN: 0008-6223. DOI: https://doi.org/10.1016/j.carbon.2005.05.006. URL: https://www.sciencedirect.com/science/article/pii/S0008622305002678.

[92] Q. Zhang et al. "High-temperature polymer conductors with self-assembled conductive pathways". In: *Composites Part B Engineering* 192 (Mar. 2020). DOI: 10.1016/j.compositesb.2020.107989.

[93] H. J. Choi et al. "Electrical percolation threshold of carbon black in a polymer matrix and its application to antistatic fibre". In: *Scientific Reports* 9.1 (2019), p. 6338. DOI: 10.1038/s41598-019-42495-1.

[94] Q. Zhang et al. "Improved electrical conductivity of polymer/carbon black composites by simultaneous dispersion and interaction-induced network assembly". In:

Composites Science and Technology 179 (2019), pp. 106–114. ISSN: 0266-3538. DOI: https://doi.org/10.1016/j.compscitech.2019.05.008. URL: https://www.sciencedirect.com/science/article/pii/S0266353818330781.

[95] A. Beiser. *Concepts of Modern Physics*. 5th. New York: McGraw-Hill, 1995. Chap. 5, p. 534. ISBN: 0071138498.

[96] MIT Student and MZB. *Lecture 20 – Quantum Tunneling of Electrons*. https://ocw.mit.edu/courses/10-626-electrochemical-energy-systems-spring-2014/21ab97bf1139670415f5338f163d7360_MIT10_626S14_Lec20.pdf. 2009.

[97] X-S. Yi, G. Wu, and D. Ma. "Property balancing for polyethylene-based carbon black-filled conductive composites". In: *Journal of Applied Polymer Science* 67.1 (1998), pp. 131–138. DOI: https://doi.org/10.1002/(SICI)1097-4628(19980103)67:1<131::AID-APP15>3.0.CO;2-4. URL: https://onlinelibrary.wiley.com/doi/abs/10.1002/%28SICI%291097-4628%2819980103%2967%3A1%3C131%3A%3AAID-APP15%3E3.0.CO%3B2-4.

[98] X-S. Yi, G. Wu, and Y. Pan. "Properties and applications of filled conductive polymer composites". In: *Polymer International* 44.2 (1997), pp. 117–124. DOI: https://doi.org/10.1002/(SICI)1097-0126(199710)44:2<117::AID-PI811>3.0.CO;2-L. URL: https://scijournals.onlinelibrary.wiley.com/doi/abs/10.1002/%28SICI%291097-0126%28199710%2944%3A2%3C117%3A%3AAID-PI811%3E3.0.CO%3B2-L.

[99] Cadence PCB Solutions. *Electrical Contact Resistance: Causes and Alleviations*. https://resources.pcb.cadence.com/blog/2023-electrical-contact-resistance-causes-and-alleviations. 2023.

[100] D. Loyd. *Contact resistance*. https://www.pentronic.se/wp-content/uploads/2020/05/20-2-contact-resistance.pdf. 2020.

[101] R. Bagherzadeh et al. "18 - Electrospun conductive nanofibers for electronics". In: *Electrospun Nanofibers*. Ed. by M. Afshari. Woodhead Publishing Series in Textiles. Woodhead Publishing, 2017, pp. 467–519. ISBN: 978-0-08-100907-9. DOI: https://doi.org/10.1016/B978-0-08-100907-9.00018-0. URL: https://www.sciencedirect.com/science/article/pii/B9780081009079000180.

[102] A. Gahoi et al. "Contact resistance study of various metal electrodes with CVD graphene". In: *Solid-State Electronics* 125 (Nov. 2016), pp. 234–239. ISSN: 0038-1101. DOI: 10.1016/j.sse.2016.07.008. URL: http://dx.doi.org/10.1016/j.sse.2016.07.008.

[103] Electrolube. *SCP: Silver Conductive Paint*. https://www.ulbrich.cz/chemical-technical-products/TDS_ELECTROLUBE_SCP_Silver_Conductive_Paint_eng.pdf. 2013.

[104] Electrolube. *SAFETY DATA SHEET SILVER CONDUCTIVE PAINT*. https://static.rapidonline.com/pdf/87-4490s_v2.pdf. 2015.

[105] GUIDELINE GEO. *What is electrode contact resistance? How can I improve contact resistance?* https://www.guidelinegeo.com/help-articles/electrode-contact-resistance/. 2022.

[106] E. K. Sichel, J. I. Gittleman, and Ping Sheng. "Electrical Properties of Carbon - Polymer Composites". In: *Journal of Electronic Materials* 11.4 (Apr. 1982), p. 709.

[107] B. Chudnovsky. "Degradation of power contacts in industrial atmosphere: silver corrosion and whiskers". In: *Proceedings of the Forty-Eighth IEEE Holm Conference on Electrical Contacts*. Feb. 2002, pp. 140–150. ISBN: 0-7803-7433-9. DOI: 10.1109/HOLM.2002.1040834.

[108] SpecialChem. *How to Enhance Polymer Properties Through Crosslinking?* Accessed: 2025-05-31. 2024. URL: https://polymer-additives.specialchem.com/tech-library/article/crosslinking.

[109] S. Soady. *The purpose of the screen and Semi-conductive layer on MV Cables*. https://www.cencepower.com/blog-posts/4-reasons-power-grids-still-distribute-ac-electricity. 2022.

[110] M. El Hasnaoui et al. "Electrical conductivity studies on carbon black loaded ethylene butylacrylate polymer composites". In: *Journal of Non-Crystalline Solids* 358.20 (2012), pp. 2810–2815. ISSN: 0022-3093. DOI: https://doi.org/10.1016/j.jnoncrysol.2012.07.008. URL: https://www.sciencedirect.com/science/article/pii/S0022309312004061.

[111] J-Z. Liang and Q-Q. Yang. "Effects of carbon black content and size on conductive properties of filled high-density polyethylene composites". In: *Advances in Polymer Technology* 37.6 (2018), pp. 2238–2245. DOI: https://doi.org/10.1002/adv.21882. URL: https://onlinelibrary.wiley.com/doi/abs/10.1002/adv.21882.

[112] J-Z. Liang and Q-Q. Yang. "Effects of carbon fiber content and size on electric conductive properties of reinforced high density polyethylene composites". In: *Composites Part B: Engineering* 114 (2017), pp. 457–466. ISSN: 1359-8368. DOI: https://doi.org/10.1016/j.compositesb.2017.02.017. URL: https://www.sciencedirect.com/science/article/pii/S1359836816328827.

[113] M. Traina, A. Pegoretti, and A. Penati. "Time-Temperature Dependence of the Electrical Resistivity of High-Density Polyethylene/Carbon Black Composites". In: *Journal of Applied Polymer Science* 106.4 (2007), pp. 2065–2074. DOI: 10.1002/app.26444.

[114] Keysight. *B2910BL Precision Source/Measure Unit*. Accessed: 2025-06-18. URL: https://www.keysight.com/us/en/product/B2910BL/precision-smu-1ch-10fa-resolution-210v-1-5a.html.

[115] C. Zhai et al. "Stress-Dependent Electrical Contact Resistance at Fractal Rough Surfaces". In: *Journal of Engineering Mechanics* 143 (May 2015), B4015001. DOI: 10.1061/(ASCE)EM.1943-7889.0000967.

[116] M. Antler. "Effect of Surface Contamination on Electric Contact Performance". In: *Treatise on Clean Surface Technology: Volume 1*. Ed. by K. L. Mittal. Boston, MA: Springer US, 1987, pp. 179–203. ISBN: 978-1-4684-9126-5. DOI: 10.1007/978-1-4684-9126-5_8. URL: https://doi.org/10.1007/978-1-4684-9126-5_8.

[117] M. Antler. "Effect of surface contamination on electric contact performance". In: *IEEE Circuits and Devices Magazine* 3.2 (1987), pp. 8–20. DOI: 10.1109/MCD.1987.6323234.

[118] X. Luo and D.D.L. Chung. "Carbon-fiber/polymer-matrix composites as capacitors". In: *Composites Science and Technology* 61.6 (2001), pp. 885–888. ISSN: 0266-3538. DOI: https://doi.org/10.1016/S0266-3538(00)00166-4. URL: https://www.sciencedirect.com/science/article/pii/S0266353800001664.

[119] C. Klason and J. Kubát. "Anomalous behavior of electrical conductivity and thermal noise in carbon black-containing polymers at Tg and Tm". In: *Journal of Applied Polymer Science* 19.3 (1975), pp. 831–845. DOI: https://doi.org/10.1002/app.1975.070190319. URL: https://onlinelibrary.wiley.com/doi/abs/10.1002/app.1975.070190319.